

# Analysis of Symbol Design Strategies for Intrapulse Radar-Embedded Communications

Justin G Metcalf, *Graduate Student Member, IEEE*,

Cenk Sahin, *Graduate Student Member, IEEE*,

Shannon D Blunt, *Senior Member, IEEE*, Muralidhar Rangaswamy, *Fellow, IEEE*

## Abstract

The design of communication symbols that may be embedded on an intra-pulse basis into the backscatter generated by a high-power, pulsed radar is considered. This framework requires the asynchronous detection of transmitted symbols in a high interference environment that degrades the capabilities of conventional intercept receivers. The impact of symbol design and filter structure upon the successful detection of covert symbols by the intended receiver and a hypothetical partially clairvoyant intercept receiver is examined.

## Index Terms

Radar clutter, Spread-spectrum communication, LPI communication, Symbol design.

## I. INTRODUCTION

As the spectrum becomes more congested, increasing attention is being paid to multi-mode systems with both sensing and communications capabilities. A prime example of this form of spectral co-habitation comes from the automotive research community [1]–[4]. In addition, the defense community is sponsoring initiatives focused on allowing radar and communication systems to coexist in the same spectrum (*e.g.* the DARPA SSPARC program [5]). This work continues in the line of [6]–[9] to examine methods of designing and detecting low probability of intercept (LPI) communication symbols that reside within radar clutter. The additional constraint of LPI requires further considerations beyond that of other multi-mode schemes.

This work was supported by the Air Force Office of Scientific Research under contract FA9550-12-1-0220.

In [6]–[9] a framework for LPI communication using masking radar clutter on an intra-pulse basis was developed and analyzed. Based on observations on symbol optimization from [9], here this concept is expanded to consider enhanced symbol and filter design strategies that incorporate the spectral shape of the clutter. In addition to the metrics used to evaluate a traditional communication system (*e.g.* bit error rate, signal-to-interference-plus-noise ratio), an LPI system must simultaneously minimize the detection probability at prospective intercept receivers, and so this attribute is likewise examined.

A spread-spectrum system is generally defined as a communication system where the information bandwidth is less than the transmission bandwidth [10]. The communication waveform may either be directly spread over a wide bandwidth or a transmission may “hop” rapidly over various frequencies. Spread-spectrum is naturally useful in an LPI context. The diversity afforded by spreading the information over a wider bandwidth provides resistance to narrowband interference and increases the difficulty for an intercept receiver to detect the transmission [10], [11]. Here we consider a form of direct spreading that is tailored to an external interference source, namely radar clutter.

The operational concept under consideration has four primary components as shown in Figure 1. First, an area is illuminated with a radar waveform, here presumed to be pulsed at an arbitrary pulse repetition frequency (PRF). Second, a transponder or tag (hereafter referred to as the “tag” for simplicity) that wishes to transmit a covert communication symbol injects an LPI symbol among the clutter (ambient reflections) generated by the radar emission. Third, a desired receiver (or multiple receivers) is/are available to detect and demodulate the covert clutter-embedded symbol and recover the information conveyed by the tag. Finally, intercept receivers may exist that attempt to detect any covert transmissions.

The tag, upon being triggered by the incident radar waveform, emits a communication symbol that is characterized such that the desired receiver(s) may readily demodulate the symbol, but the intercept receiver cannot detect the presence of the embedded signal among the radar clutter. By transmitting communication symbols on a per-pulse basis, the tag realizes a data rate on the order of the PRF. The radar and desired receiver may be colocated or separated, where the former also enables the tag to make use of time-reversal to exploit multipath for space-time focusing [9]. Note that this covert communication framework developed in [6]–[9] is general and admits any number of transmitting tags as long as the respective symbols do not completely overlap. However, for notational and analytical convenience here we consider the case of a single

transmitting tag.

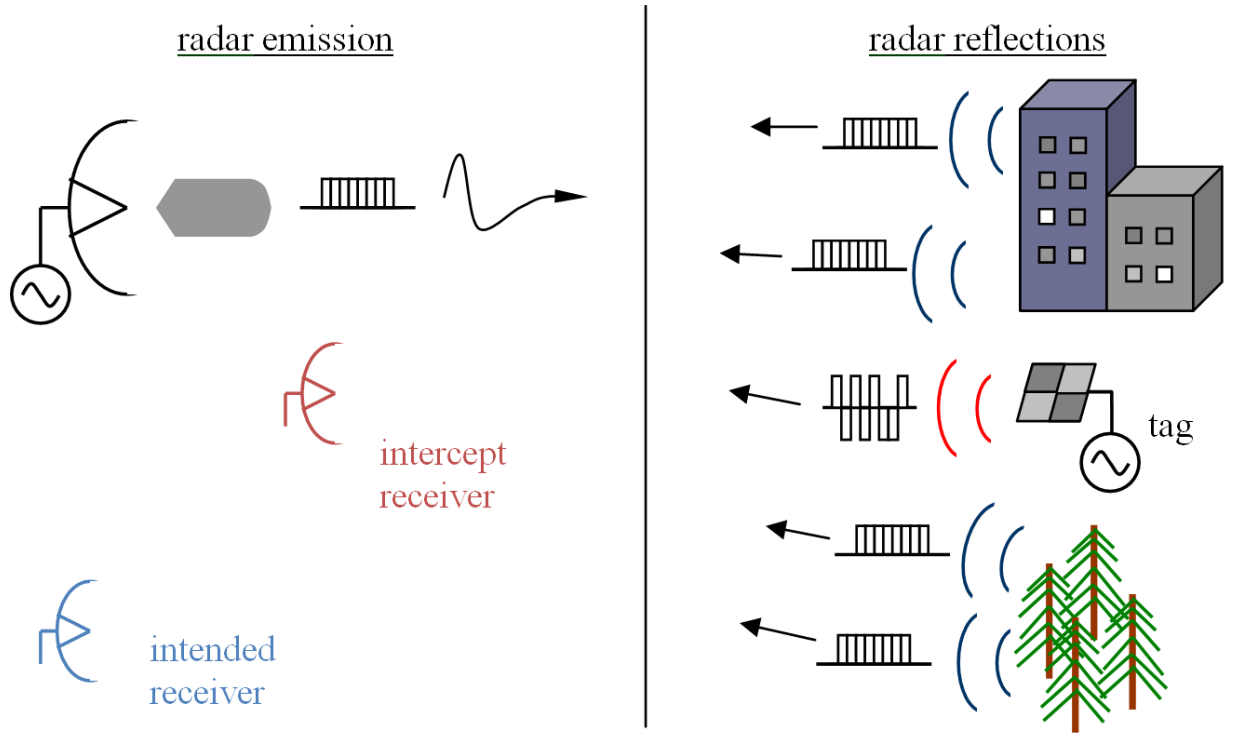


Fig. 1: Generic radar-embedded communications system

It is important to note that the framework under consideration inherently imposes several practical trade-offs and constraints on symbol and receiver design. The constraints with the greatest influence are summarized in Table I and are necessarily interrelated and driven by the dual goals of maximizing the data rate through the communication system while minimizing the probability of intercept. The presence of radar clutter offers an opportunity to construct LPI communication symbols. However, constructing communication symbols to take advantage of the masking radar clutter necessarily limits the symbol design choices available. For example, to maintain LPI the symbols are designed to be correlated with the waveform-induced clutter and occupy a similar temporal and spectral footprint via subspace projection. As such, the symbols occupy a linear space with limited degrees of freedom (DOF) and must be transmitted in a burst mode triggered by the incident radar illumination, such that the repetition rate of the burst mode is constrained to the requirements of the illuminating radar rather than any characteristics desired by the communication receivers. In practice, the surrounding clutter is unknown and the radar waveform must be determined from the observed illumination, which may contain multipath and

TABLE I: Practical design constraints for intrapulse radar-embedded communications

1. Radar, tag, and desired receiver are not synchronized.
2. Symbols must be determined independently at the tag and desired receiver based on the observed radar illumination (possible timing uncertainty and multipath differences).
3. The surrounding clutter structure is not known exactly, though it can be viewed as a random signal convolved with the radar waveform.
4. Symbols are designed to be partially correlated with the clutter but still separable from one another on receive.
5. Symbols have temporal and spectral footprint commensurate with the radar waveform.
6. Symbol design must occur in a reasonable time frame (while radar illumination persists).

possess relative sample timing differences between the tag and desired receiver. Therefore, as the symbols are dynamically generated based on the characteristics of the radar illumination, the symbol and receive filter designs should be robust to mismatch between the tag and receiver. In addition, the receiver must be able to synchronize with the received symbol without aid of pilot symbols or an external control channel. Finally, the intercept receiver must be considered. Quantifying the LPI nature of a given transmission scheme is not a well-defined problem [12]. Therefore, a hypothesized "worst case" bound on intercept receiver (IR) performance is employed here in which the IR metric incorporates some clairvoyant knowledge regarding the possible embedded symbols.

The observations made in [6], [7], [9] have developed and informed the constraints in Table I. Here we use these prior observations to define and analyze alternative symbol design structures with the goal of gaining insight into what factors impact overall performance under the given constraints. Specifically, the well-known waterfilling approach is examined along with the impact of shaping according to the spectral response of the radar illumination. The proposed symbol designs are not intended to represent the optimal symbols but instead to highlight attractive symbol attributes within the practical constraints of the radar-embedded communication problem. As the approaches presented here do not alter the fundamental subspace projection approach of [6]–[9], the robustness to clutter covariance estimation mismatch of the original approaches is maintained. However, while the computational complexity of the approach must be considered

(i.e. point 6 of Table I), the analysis of the computational complexity is beyond the scope of this work.

The remainder of the paper is organized as follows. In Section II we examine new designs for intra-pulse radar-embedded symbols, using the classic direct sequence spread spectrum (DSSS) and previous schemes from [7], [9] for comparison. Section III then briefly reviews the two-stage Neyman-Pearson (NP) receiver structure from [9]. In Section IV the proposed symbols are examined in conjunction with three filter structures, and the processing gain relative to an energy detector (i.e. total power radiometer based intercept receiver) is examined. Finally, Section V evaluates the probability of detection by the partially clairvoyant intercept receiver and by the desired receiver along with bit error rate.

## II. LOW PROBABILITY OF INTERCEPT COMMUNICATION SYMBOL DESIGN

The design of the communication symbols is constrained by the factors discussed in Table I. Therefore, we consider a general class of symbols with desirable properties to meet the design criteria discussed in Section I. Each of these symbol design methods has been informed by the developments of [6], [7], [9]. First, a traditional spread-spectrum symbol design is presented to provide a performance baseline that does not account for the presence of masking radar clutter. Then, to examine the impact of spectral shaping to better fit the surrounding clutter (relative to the original dominant projection (DP) approach [7]) the spectral roll-off of the radar illumination is factored into the symbol design. In addition, the well-known waterfilling scheme is examined within this clutter masking context, with a modified version proposed that also addresses the desired LPI attribute.

For the communication symbols to be LPI, they are designed to be partially correlated with the clutter, yet possess a structure that may be used by the desired receiver to separate the symbols from the clutter. Let  $N$  be the number of discrete samples required to characterize fully the radar waveform based on Nyquist sampling according to the 3 dB bandwidth. Define  $M$  as an "oversampling" factor that is used to control the amount of additional spreading the communication symbols undergo with relation to the radar 3 dB bandwidth. The continuous radar waveform is denoted  $s(t)$  and its discrete oversampled representation is the length  $NM$  vector  $\mathbf{s}$ .

As shown in [7] and [9], the ambient signal generated by the collection of radar reflections and collected at an arbitrary receiver can be expressed as

$$\mathbf{y} = \mathbf{S}\mathbf{x} + \mathbf{u} \quad (1)$$

where  $\mathbf{u}$  is a  $NM \times 1$  vector of complex additive Gaussian noise and  $\mathbf{S}\mathbf{x}$  is the discrete convolution between the radar waveform and the arbitrary clutter process  $\mathbf{x}$ , which is unknown. This discrete convolution is performed using the  $NM \times (2NM - 1)$  Toeplitz matrix  $\mathbf{S}$  that consists of delay shifts of the radar waveform and is expressed as

$$\mathbf{S} = \begin{bmatrix} s_{NM-1} & s_{NM-2} & \cdots & s_0 & 0 & \cdots & 0 \\ 0 & s_{NM-1} & \cdots & s_1 & s_0 & \cdots & 0 \\ \vdots & \vdots & \ddots & \vdots & \vdots & \ddots & \vdots \\ 0 & 0 & \cdots & s_{NM-1} & s_{NM-2} & \cdots & s_0 \end{bmatrix}. \quad (2)$$

The normalized correlation of the clutter response admits the eigen decomposition [7], [9]

$$\begin{aligned} \frac{1}{\sigma_x^2} E[(\mathbf{S}\mathbf{x})(\mathbf{S}\mathbf{x})^H] &= \frac{1}{\sigma_x^2} \mathbf{S} E[\mathbf{x}\mathbf{x}^H] \mathbf{S}^H \\ &= \mathbf{S}\mathbf{S}^H \\ &= \mathbf{V}\mathbf{\Lambda}\mathbf{V}^H \end{aligned} \quad (3)$$

where  $\mathbf{\Lambda}$  is a diagonal matrix of eigenvalues in descending order associated with the eigenvectors in  $\mathbf{V}$  and the clutter process is assumed to be uncorrelated in range with equal variance at each sample. This assumption reflects the lack of knowledge regarding the correlation of surrounding clutter and could readily be modified if such knowledge were available (*e.g.* if additional masking clutter were artificially generated as suggested in [7]). The methods considered below all operate on a subspace basis, reducing the impact of mismatch between covariance matrix estimates due to synchronization difference [7] or multipath [9].

For simplicity, we assume that the radar waveform is constant modulus and normalized such that  $\mathbf{s}^H \mathbf{s} = 1$ . Therefore,

$$\begin{aligned} \text{tr}\{\mathbf{S}\mathbf{S}^H\} &= \sum_{i=1}^{NM} \mathbf{s}_i^H \mathbf{s}_i = NM \\ &= \text{tr}\{\mathbf{\Lambda}\} = \text{tr}\{\mathbf{V}\mathbf{\Lambda}\mathbf{V}^H\} \end{aligned} \quad (4)$$

where the equality of the first and last terms is taken from (3).

### A. Direct Sequence Spread Spectrum (DSSS)

To provide a performance baseline in which the masking clutter is not utilized, first consider a conventional communication system with a total transmit energy constraint  $\gamma$ . However, instead of allocating transmitted power to, for example, subchannels within an orthogonal-frequency division (OFDM) framework, here power is allocated according the eigenvectors of the overall clutter-plus-noise space induced by the radar illumination. The classical direct sequence spread spectrum (DSSS) approach spreads the symbol energy uniformly over the transmit bandwidth [10]. Therefore, an eigenspace based DSSS approach would be to assign a uniform transmit power of  $\frac{\gamma}{NM}$  to each "eigenchannel" (eigenvector), so the  $k^{th}$  DSSS symbol can be defined as

$$\begin{aligned} \mathbf{c}_{\text{DSSS},k} &= \frac{\gamma}{NM} \mathbf{V}^H \mathbf{b}_k \\ &= \frac{\gamma}{NM} \mathbf{q}_k. \end{aligned} \quad (5)$$

In (5),  $\mathbf{b}_k$  is an  $NM \times 1$  pseudo-random spreading vector known to both the tag and any desired receivers, and we have defined

$$\mathbf{q}_k \doteq \mathbf{V}^H \mathbf{b}_k \quad (6)$$

to be the transformed spreading vector. The approach of (5) differs from traditional DSSS schemes in that the spreading vectors provide an alphabet of communication symbols rather than distinguishing between users, as is the case in a traditional code-division multiple access (CDMA) scheme.

### B. Dominant Projection (DP)

One possible method to mitigate the impact of the clutter on communication performance is to allocate no transmit power to eigenchannels associated with a strong clutter response. The eigenvectors  $\mathbf{V}$  in (3) can be partitioned into subspaces associated with the  $m$  largest (dominant - D) and  $NM - m$  smallest (non-dominant - ND) eigenvalues [7], [9] as

$$\mathbf{V} \mathbf{\Lambda} \mathbf{V}^H = \left[ \mathbf{V}_D \mid \mathbf{V}_{\text{ND}} \right] \left[ \begin{array}{c|c} \mathbf{\Lambda}_D & \mathbf{0} \\ \hline \mathbf{0} & \mathbf{\Lambda}_{\text{ND}} \end{array} \right] \left[ \begin{array}{c} \mathbf{V}_D^H \\ \hline \mathbf{V}_{\text{ND}}^H \end{array} \right]. \quad (7)$$

A logical division of dominant and non-dominant subspaces is to designate the dominant subspace to be  $m = N$  (*i.e.* the time-bandwidth dimensionality occupied by the radar waveform) and the non-dominant subspace to be the eigenvectors associated with the remaining  $NM - N$  eigenvalues [7]. However, varying the size of dominant and non-dominant subspaces offers more freedom

with which to design the communication symbols, thus allowing for optimization [9]. The method of symbol design in [7], [9] formed the projection matrix

$$\begin{aligned}\mathbf{A} &= \mathbf{I} - \mathbf{V}_{D,m} \mathbf{V}_{D,m}^H \\ &= \mathbf{V}_{ND,m} \mathbf{V}_{ND,m}^H\end{aligned}\quad (8)$$

where the subscript  $m$  indicates the number of dominant eigenvectors in  $\mathbf{V}_{D,m}$ . The  $k^{th}$  dominant projection (DP) communication symbol is then formed as

$$\begin{aligned}\mathbf{c}_{DP,k} &= \beta_{DP,m}^{1/2} \mathbf{A} \mathbf{b}_k \\ &= \beta_{DP,m}^{1/2} \mathbf{V}_{ND,m} \mathbf{V}_{ND,m}^H \mathbf{b}_k \\ &= \beta_{DP,m}^{1/2} \mathbf{V}_{ND,m} \mathbf{q}_{ND,k}\end{aligned}\quad (9)$$

where  $\beta_{DP,m}^{1/2}$  is a scaling factor introduced here to enable a fair comparison between the different symbol design strategies, and  $\mathbf{q}_{ND,k} = \mathbf{V}_{ND,m}^H \mathbf{b}_k$  is the  $(NM - m) \times 1$  transformed spreading vector associated with the non-dominant subspace. For  $\|\mathbf{b}_k\|^2 = 1$  and  $\mathbf{b}_k$  an  $NM \times 1$  vector, we find [9]

$$\begin{aligned}|b_{k,i}|_{\text{avg}}^2 &= |q_{k,i}|_{\text{avg}}^2 \\ &\approx \frac{1}{NM}\end{aligned}\quad (10)$$

since  $\mathbf{V}$  is a unitary transform.

The expected transmitted signal power of (9) is

$$\begin{aligned}S &= \|\mathbf{c}_{DP,k}\|^2 = \mathbf{c}_{DP,k}^H \mathbf{c}_{DP,k} \\ &= \left( \beta_{DP,m}^{1/2} \mathbf{q}_{ND,k}^H \mathbf{V}_{ND,m}^H \right) \left( \beta_{DP,m}^{1/2} \mathbf{V}_{ND,m} \mathbf{q}_{ND,k} \right) \\ &= \beta_{DP,m} \mathbf{q}_{ND,k}^H \mathbf{q}_{ND,k} \\ &\approx \beta_{DP,m} \sum_{i=m+1}^{NM} |q_{k,i}|_{\text{avg}}^2 \\ &= \frac{\beta_{DP,m} (NM - m)}{NM}.\end{aligned}\quad (11)$$

To allow for a constant transmit energy of  $\gamma$ , regardless of the dimensionality  $m$  of the dominant subspace, examination of (11) yields a scaling factor of

$$\beta_{DP,m} = \frac{\gamma NM}{NM - m}.\quad (12)$$

The DP method of [7], [9] takes advantage of the clutter response structure imposed by the radar waveform to shape communication symbols that are correlated with, yet separable from, the clutter assuming knowledge of  $\mathbf{b}_k$ . In addition, by using the non-dominant subspace *as a whole* (i.e. as opposed to individual non-dominant eigenvectors) the symbols generated by the DP method are relatively unchanged even when the observed radar waveform is sampled with a relative timing offset between the tag and desired receiver or is corrupted by multipath [7], [9]. Notice that at the extreme case of  $m = 0$ , due to the orthonormal nature of eigenvectors the DP method becomes analogous to the classical DSSS method of Section II-A. However, the information contained within the eigenvalues  $\Lambda$  is ignored with the DP approach. In contrast, we now consider the impact of incorporating the eigenvalues  $\Lambda$  to further shape the LPI symbols according to the clutter spectral response.

### C. Shaped Dominant Projection (SDP)

The DP symbols of (9) allocate power evenly over the entire non-dominant subspace which, as shown in [9], impacts the optimal dimensionality to ensure that LPI is maintained. The eigenvalues of (3) provide information on the relative clutter-plus-noise power at each eigenchannel. In particular, the spectral shape of the clutter-plus-noise response exhibits a "rolloff" between the 3 dB bandwidth of the radar waveform and the noise floor. By incorporating knowledge of the eigenvalues into the symbol design, the spectrum occupied by the communication symbols can more closely imitate the spectral shape of the rolloff and thereby improve LPI performance.

Define the  $k^{\text{th}}$  shaped dominant projection (SDP) symbol as

$$\begin{aligned} \mathbf{c}_{\text{SDP},k} &= \beta_{\text{SDP}}^{1/2} \mathbf{V}_{\text{ND},m} \Lambda_{\text{ND},m}^{1/2} \mathbf{V}_{\text{ND},m}^H \mathbf{b}_k \\ &= \beta_{\text{SDP}}^{1/2} \mathbf{V}_{\text{ND},m} \Lambda_{\text{ND},m}^{1/2} \mathbf{q}_{\text{ND},k}, \end{aligned} \quad (13)$$

with scaling factor

$$\beta_{\text{SDP}} = \frac{\gamma NM}{\text{tr}\{\Lambda_{\text{ND},m}\}} \quad (14)$$

to ensure the overall symbol energy is  $\gamma$ . Compared to the DP symbol in (9), the SDP symbol in (13) includes the  $\Lambda_{\text{ND}}$  term that serves to shape the symbol spectrum to match that of the radar clutter (in the roll-off region since only the non-dominant portion is addressed).

#### D. Shaped Waterfilling

A well-known method to shape the power across a set of channels is to assign power according to the inverse of the associated gains/losses (otherwise known as "waterfilling" [13]). Applying this principle to the present symbol design problem would mean that eigenvectors associated with the strongest clutter response would be transmitted at the lowest power and vice versa. Thus, a  $k^{\text{th}}$  waterfilling (WF) symbol could be defined as

$$\begin{aligned} \mathbf{c}_{\text{WF},k} &= \beta_{\text{WF}}^{1/2} \mathbf{V} \mathbf{\Lambda}^{-1/2} \mathbf{V}^H \mathbf{b}_k \\ &= \beta_{\text{WF}}^{1/2} \mathbf{V} \mathbf{\Lambda}^{-1/2} \mathbf{q}_k \end{aligned} \quad (15)$$

where  $\beta_{\text{WF}}$  is the normalizing scale factor

$$\beta_{\text{WF}} = \frac{\gamma NM}{\text{tr} \{ \mathbf{\Lambda}^{-1} \}}. \quad (16)$$

For the WF approach, the eigenchannels with the greatest allocated power will coincide with the lowest clutter-plus-noise channel response. However, by transmitting the greatest power on the eigenchannel with the lowest interference, the LPI performance would clearly suffer. As such, consider a *partitioned* approach that combines waterfilling with the previous symbol shaping. Define the partitioned eigenvalue matrix for this hybrid shaped waterfilling formulation as

$$\mathbf{\Lambda}_{\text{P},m} = \left[ \begin{array}{c|c} \mathbf{\Lambda}_{\text{D},m}^{-1} & \mathbf{0} \\ \hline \mathbf{0} & \mathbf{\Lambda}_{\text{ND},m} \end{array} \right] \quad (17)$$

where the dimensionality  $m$  still provides an optimizable parameter as in [9]. The  $k^{\text{th}}$  shaped waterfilling (SWF) communication symbol is thus

$$\begin{aligned} \mathbf{c}_{\text{SWF},k} &= \beta_{\text{SWF}}^{1/2} \mathbf{V} \mathbf{\Lambda}_{\text{P},m}^{1/2} \mathbf{V} \mathbf{\Lambda}^{-1/2} \mathbf{q}_k \\ &= \beta_{\text{SWF}}^{1/2} \mathbf{V} \mathbf{\Lambda}_{\text{P},m}^{1/2} \mathbf{q}_k \end{aligned} \quad (18)$$

where

$$\beta_{\text{SWF}} = \frac{\gamma NM}{\text{tr} \{ \mathbf{\Lambda}_{\text{P},m} \}}. \quad (19)$$

Note that at the extreme of  $m = NM$ , the SWF symbol design subsumes the WF symbol design. Therefore, from this point forward we only consider the more general SWF approach.

Taking inspiration from the classical waterfilling approach to maximizing capacity under a power constraint [13], one could discard the eigenchannels associated with the greatest clutter response. Such an approach naturally leads to the shaped DP method, defined in (13). Therefore,

the SDP and SWF symbol designs represent classes of symbols that should provide insight into preferable structures based on the many practical implementation constraints.

### *E. Spectral Content of LPI Symbols*

Spectrally, the environment contains contributions from the clutter as well as ambient thermal noise. Assuming the clutter power is much greater than the noise power, the clutter subspace can be defined as the subspace spanned by the first  $N$  eigenvectors (*i.e.* the time-bandwidth product of the radar waveform). The noise subspace is then spanned by the remaining  $NM - N$  eigenvectors. As the dominant and non-dominant subspaces have been defined generally, with boundary given by  $m$ , the resultant communication symbols have different forms depending on the formation of the projection matrices with relation to the noise and clutter subspaces. Here we illustrate this dependence for several choices of  $m$  by showing the average spectral content of the various symbol design methods. This examination is meant to provide an intuition to the response of each symbol design method and further justification for each method used.

In all cases,  $10^6$  communication symbols were formed from random-phase spreading vectors. The spectral content of these symbols were determined and averaged. The radar waveform is a linearly frequency modulated (LFM) waveform [14] with a time-bandwidth product of  $N = 64$ , oversampled by a factor of  $M = 2$ . We use the DSSS method as a baseline, and additionally show the average clutter-plus-noise response (denoted as R+N) with a clutter-to-noise (CNR) of 30 dB. All communications symbols are constrained to have a constant power constraint of  $\gamma = 1$ , providing a 0 dB signal-to-noise ratio (SNR).

First, Figure 2 illustrates the average spectral content when the dominant subspace is set to be half of the waveform time-bandwidth product. For the parameters given above, this condition occurs when  $m = 32$ . The DP method results in nulls at the dominant eigenchannels (which coincide with the peaks in the clutter response), but to maintain the constant transmit power the non-dominant eigenchannels are transmitted at a higher power than the DSSS symbol (which has a uniform transmit power over all eigenchannels). This scaling causes the DP method to have the largest transmit power in the noise subspace of all the symbol design methods under consideration. In contrast, the SDP symbols display a rolloff in the eigenchannels associated with the transition from clutter to noise subspace that mirrors the clutter-plus-noise spectrum. Also, the SDP symbols place shallower nulls at the dominant eigenchannels, and assign additional power (relative to the DP method) to the eigenchannels that are in the clutter subspace but

are considered (through the value of  $m$ ) to be in the non-dominant subspace. Finally, the SWF symbol produces a spectrum between the extremes of the DP and SDP methods. As the dominant eigenchannels are weighted by the inverse of their eigenvalues, rather than projected out, the spectral response is shallowly suppressed rather than nulled. Therefore, slightly more power is transmitted in the clutter subspace by the SWF symbols than the SDP symbols.

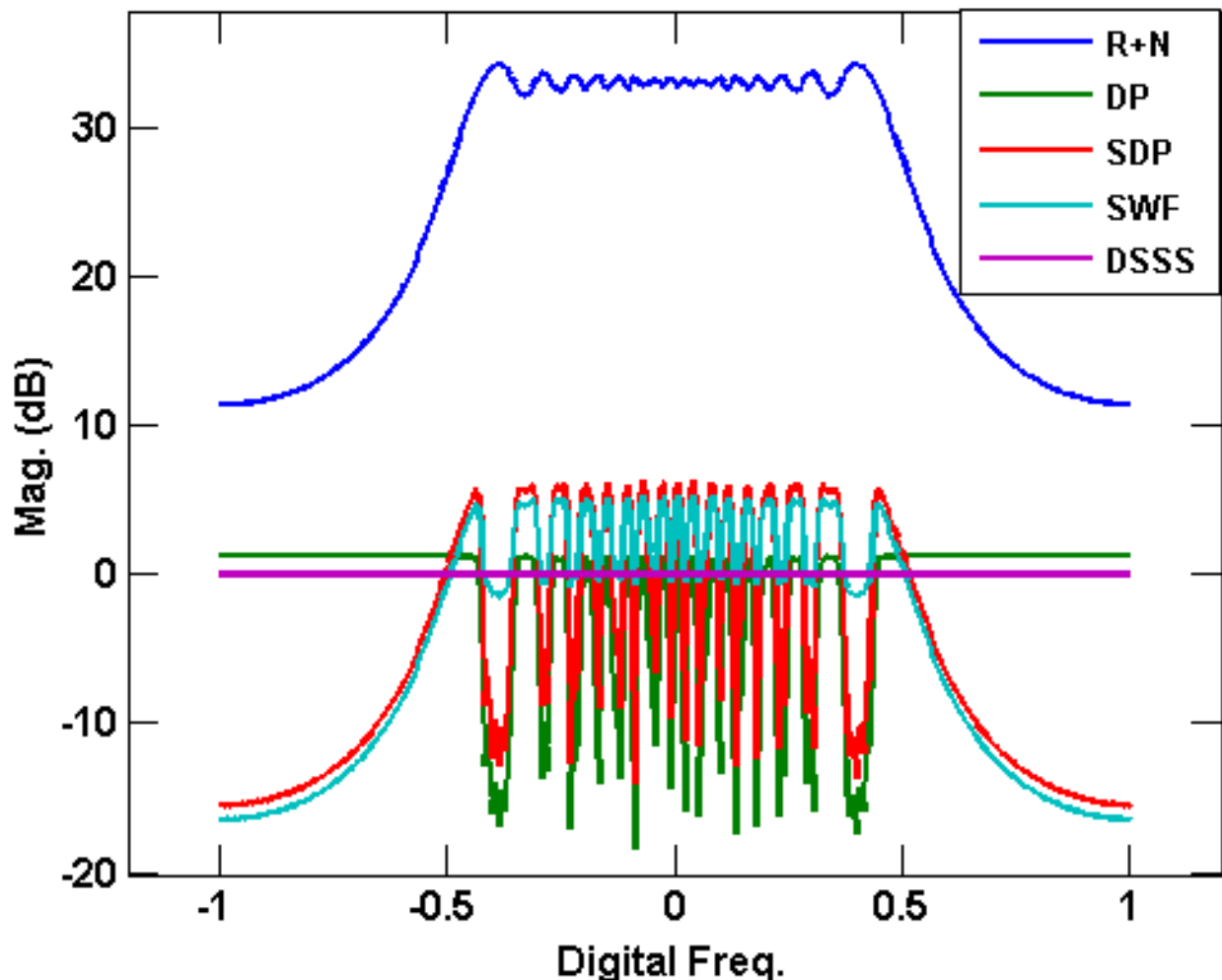


Fig. 2: Spectral content for radar-embedded communication symbols,  $m = 32$ .

Next, Figure 3 depicts the case where  $m = N = 64$ . In other words, the clutter subspace is considered to be the dominant subspace and the noise subspace is the non-dominant subspace (for  $M = 2$ ). Once more, the SWF symbol produces a lower response in the noise subspace than either the DP or SDP method and allocates the most power of all symbol design methods to the clutter subspace. However the SDP method allows for the symbol to allocate power where

there is spectral bleeding between the clutter and noise subspaces, which results in more power allocated to the clutter subspace and less power at the extremes of the noise subspace relative to the DP method.

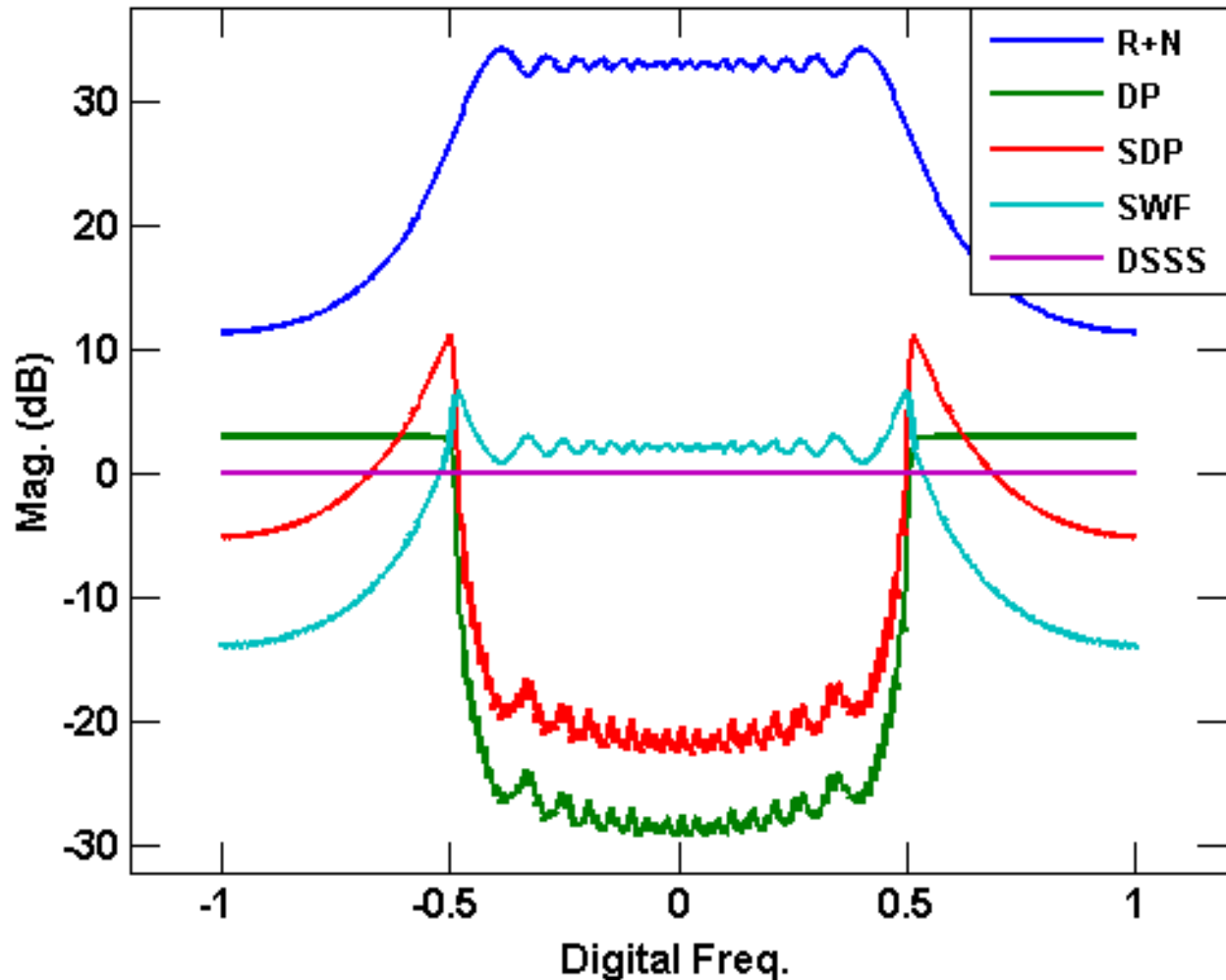


Fig. 3: Spectral content for radar-embedded communication symbols,  $m = 64$ .

Next, Figure 4 shows the spectral response when  $m = 96$ , or when the non-dominant subspace is set to be equal to half of the noise subspace (the half associated with the  $(NM - N)/2$  lowest eigenvalues). Notice that the relative equality of the eigenvalues and the scaling factors cause the DP and SDP methods to occupy similar regions of the spectrum. However, for the SWF symbols the inversion of the dominant eigenvalues in (17) causes a large spectral response when noise eigenvalues are considered to be part of the dominant subspace. This inversion causes a peak response  $\approx 2$  dB greater than the peak response of the SDP symbol for the same value of

$m$ . That said, while the peak value of the SWF symbol is greater than the DP or SDP symbol, the extreme of the noise subspace is allocated  $\approx 16$  dB less transmit power than DP or SDP symbols.

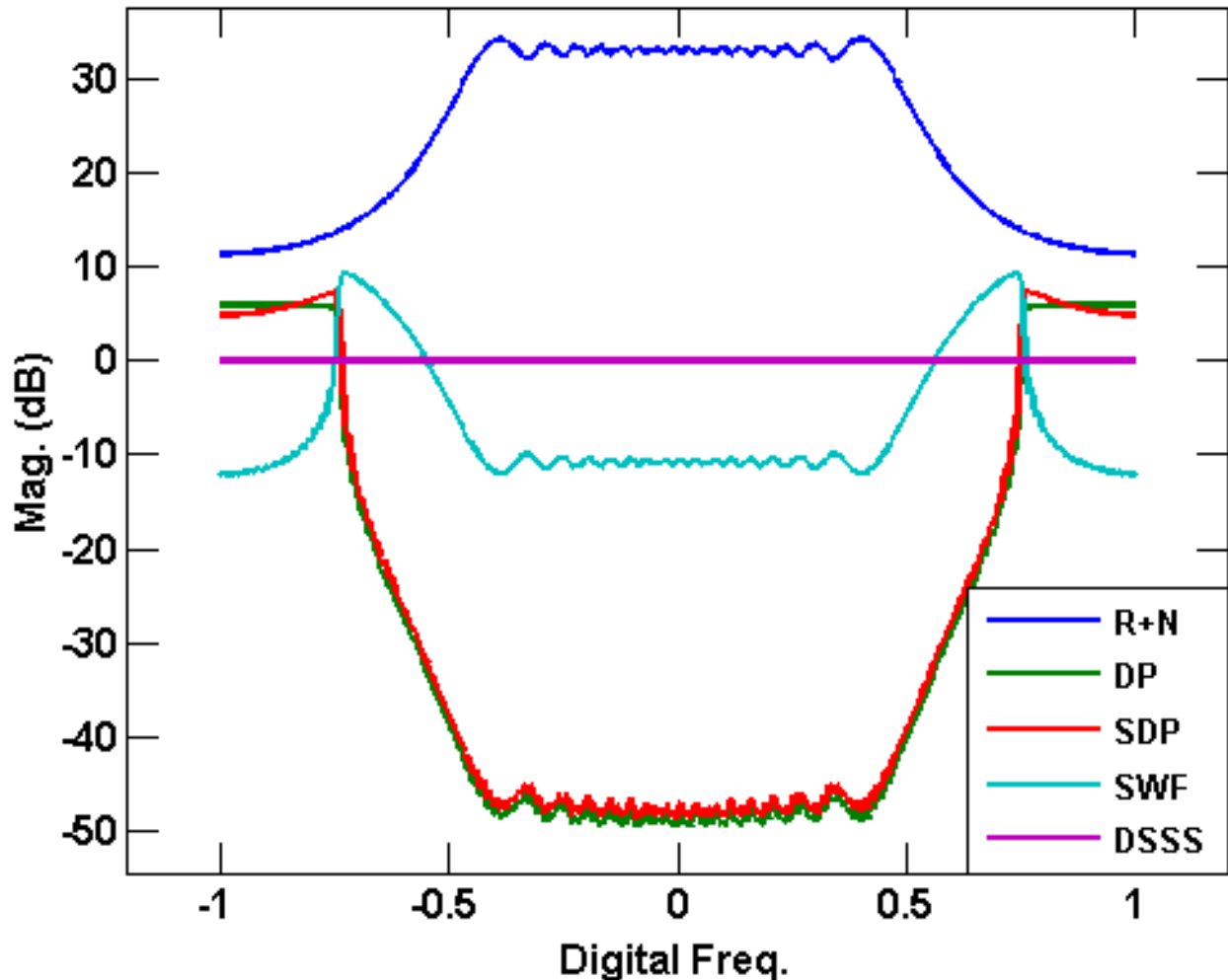


Fig. 4: Spectral content for radar-embedded communication symbols,  $m = 96$ .

Finally, Figure 5 examines the spectral response of the symbols when the dominant subspace is set to 126, leaving 2 eigenvectors for the non-dominant subspace. The SDP and DP spectral response are now approximately equivalent. In addition, the constant power constraint results in all of the power for the DP/SDP symbols to be allocated to the subspace associated with the two smallest eigenvalues. Therefore, the transmitted symbol power is observed to spike in the region of the spectrum with the least amount of masking clutter. While advantageous from an interference avoidance perspective, these symbols are clearly not LPI. Notice the contrast between

the nulling of the dominant subspace by the DP/SDP techniques and the inverse approach used by the SWF. This contrast was observed in Figure 4, but is even more apparent in Figure 5. Weighting the dominant subspace with the associated inverse eigenvalues results in a greater amount of transmit energy allocated to the clutter subspace than the DP and SDP methods allow. This energy allocation of SWF prevents the high power "spike" associated with the DP and SDP symbols. However, when compared to Figure 4 the SWF symbols allocate an increasing amount of energy to the tails of the spectral rolloff. Therefore, as SWF approaches the traditional waterfilling approach, the power levels associated with the noise subspace are all greater than the power levels used by the DSSS symbol design. Therefore, the increased energy associated with frequencies away from the masking clutter causes the symbol to become more vulnerable to interception by intercept receiver methods based on energy detection [11].

### III. SYMBOL DETECTION

Once the symbol has been transmitted by the tag, one or more intended receivers must reliably detect and decode the transmission. As the intended receivers do not know *a priori* when the transmission begins, symbol detection must be performed asynchronously. An observation interval is defined as the length  $NM$  vector  $\mathbf{y}(\ell) = [y(\ell) \ y(\ell - 1) \ \dots \ y(\ell - NM + 1)]^T$  obtained by the receiver A/D. The receiver searches for a communication symbol over an observation interval  $\gg NM$  [9]. Due to the nature of the embedded symbol, the receiver must perform filtering to suppress the clutter and coherently integrate the energy of the symbol (if present). The receive filter bank is composed of  $K$  filters denoted  $\mathbf{w}_k$  corresponding to each possible symbol.

The receiver generates a set of outputs from the filter bank, defined as  $z_{y,k}(\ell) = \mathbf{w}_k^H \mathbf{y}(\ell)$  [9]. The output of each filter forms a set  $\{z_{y,1}(\ell) \ z_{y,2}(\ell) \ \dots \ z_{y,K}(\ell)\}$ , for a collection of time samples indexed by  $\ell$ . This set is sorted to determine the magnitude of the greatest response for each filter, with the collection of maximum magnitudes providing the location in the observation interval for which each symbol has the highest probability of being present. Subsequently, the maximum over this set of  $K$  values, denoted  $|z_{y,\max}^{(k)}|$ , is the magnitude of the most likely symbol to be present over the observation interval [9].

Formally, the receive filtering may be formulated as a multiple hypothesis test where the  $K+1$  hypotheses are expressed as

$$\mathcal{H}_0 : \mathbf{y} = \mathbf{S}\mathbf{x} + \mathbf{u}$$

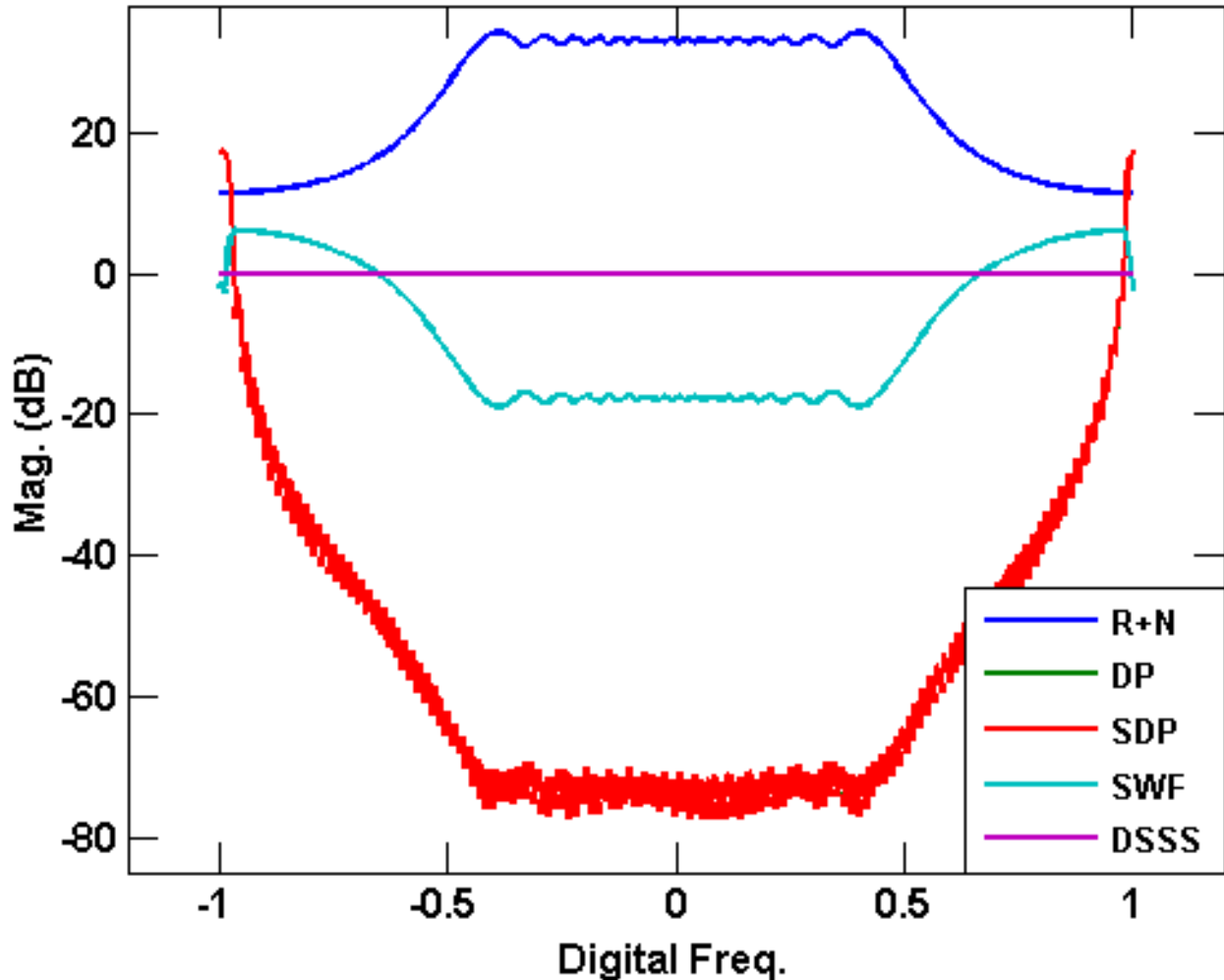


Fig. 5: Spectral content for radar-embedded communication symbols,  $m = 126$ . SWF now closely approximates standard waterfilling.

$$\mathcal{H}_k : \mathbf{y} = \mathbf{S}\mathbf{x} + \alpha\mathbf{c}_k + \mathbf{u} \quad \text{for } k = 1, 2, \dots, K. \quad (20)$$

Hypothesis  $\mathcal{H}_k$  corresponds to the  $k$ th symbol being received, with  $\alpha$  an unknown complex scaling factor that subsumes the transmitted symbol power  $\gamma$  and  $\mathcal{H}_0$  is the null hypothesis (no symbol present). The maximum output from the  $k$  filters is

$$|z_{y,\max}^{(k)}| = \max_{k,\ell} |z_{y,k}(\ell)| \quad (21)$$

such that the most likely symbol to be present in the observation interval is

$$\hat{k} = \arg \max_{k,\ell} |z_{y,k}(\ell)|. \quad (22)$$

To account for the null hypothesis and control the probability of false alarm, the receiver may use the filter outputs of the  $K - 1$  rejected symbols ( $k \neq \hat{k}$ ) to characterize the filtered clutter and noise [9]. This characterization is then used to form a threshold  $\mathcal{T}$  based on an acceptable probability of false alarm. If  $|z_{y,\max}^{(k)}| > \mathcal{T}$ , then the receiver decides that the  $\hat{k}$ th symbol is present in the observation interval. Otherwise, the receiver decides that no communication symbol is present. This two-stage process uses an adaptive Neyman-Pearson approach [15].

While the clutter process  $x(t)$  is not known, we can assume that it is zero mean. If this assumption is met, the central limit theorem causes the linear transformation of  $\mathbf{S}\mathbf{x}$  from (1), followed by the filtering  $\mathbf{w}_k^H \mathbf{y}(\ell)$ , to result in complex Gaussian distributed samples. Therefore, the filter output  $|z_{y,k}(\ell)|$  can be approximated as independent and identically distributed Rayleigh samples. If no symbol is present, the probability of false alarm is given by the probability that the maximum value of  $(K - 1)L$  Rayleigh random variables exceeds a threshold. Under the assumption that the  $(K - 1)L$  samples are IID, the probability of false alarm is found from the cdf of the Rayleigh distribution as [15]

$$\begin{aligned} F_Z(z; \sigma) &= \left[ 1 - \exp \left\{ -\frac{z^2}{2\sigma^2} \right\} \right]^{(K-1)L} \Bigg|_{z=\mathcal{T}} \\ &= 1 - P_{\text{fa}}. \end{aligned} \quad (23)$$

By rearranging, the Neyman-Pearson threshold  $\mathcal{T}$  for the detector is then

$$\mathcal{T} = \sqrt{-2\sigma_z^2 \ln \left[ 1 - (1 - P_{\text{fa}})^{\frac{1}{(K-1)L}} \right]} \quad (24)$$

where  $\sigma_z$  is the Rayleigh scale parameter. The maximum likelihood estimator (MLE) of  $\sigma_z$  is given as [16]

$$\hat{\sigma} = \sqrt{\frac{1}{2(K-1)L} \sum_{j=1, j \neq \hat{k}}^K \sum_{\ell=1}^L |z_{y,j}(\ell)|^2}. \quad (25)$$

The MLE in (25) is biased and the expected value can be expressed as [16]

$$E[\hat{\sigma}] \approx \sigma_z \left( 1 - \frac{1}{8(K-1)L} \right). \quad (26)$$

However, (26) asymptotically approaches an unbiased estimate and  $(K - 1)L$  can be assumed to be large.<sup>1</sup> The final detector output is

$$\text{symbol decision} = \begin{cases} k^{\text{th}} \text{ symbol,} & \text{if } |z_{y,\max}^{(k)}| > \mathcal{T} \\ \text{no symbol,} & \text{otherwise} \end{cases} \quad (27)$$

and the overall two-stage detector is summarized in Figure 6.

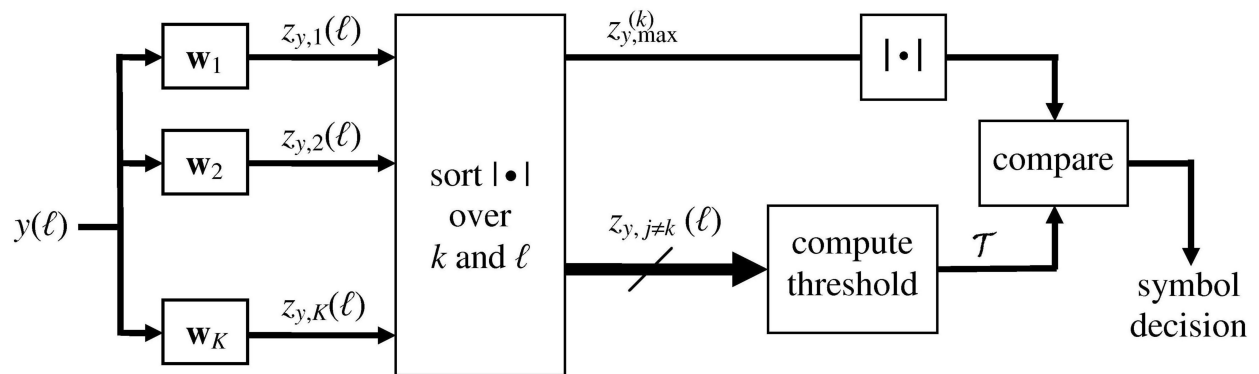


Fig. 6: Two stage Neyman-Pearson detector [9]

#### IV. RECEIVE FILTERING

The approach to receive filtering in [7] drew inspiration from the rich spread-spectrum literature, as well as noting the special circumstances inherent to radar-embedded communications. Due to the high transmit power used by a typical radar system, the received clutter power is assumed to be large relative to the noise so that the interference structure can be estimated. With this assumption in hand, [9] used a diagonally-loaded decorrelating filter [17], [18], with the filter corresponding to the  $k^{\text{th}}$  symbol given as

$$\mathbf{w}_k = (\mathbf{S}\mathbf{S}^H + \lambda_{m+1}\mathbf{I})^{-1} \mathbf{c}_k \quad \text{for } k = 1, 2, \dots, K, \quad (28)$$

where the diagonal loading term  $\lambda_{m+1}$  is the largest non-dominant eigenvalue from (7). The diagonal loading was introduced for mathematical convenience in the analysis of the filter performance and to prevent noise enhancement effects.

<sup>1</sup>Note that in [9], the threshold dependence was erroneously given as the maximum of a single Rayleigh random variable, rather than  $(K - 1)L$  samples. However, the Rayleigh distribution possesses a light tail. For the examples in [9] the threshold should be only  $\sim 1.2$  dB higher to meet the desired  $P_{\text{fa}}$  of  $10^{-5}$ .

To examine the performance of the decorrelating filter of (28), the analysis conducted in [9] derived the processing gain

$$\Delta = \frac{\text{SINR}_o}{\text{SINR}_i}, \quad (29)$$

where  $\text{SINR}_i$  corresponds to the incident communication signal, clutter, and noise and  $\text{SINR}_o$  results from receive filtering. The processing gain for the DP symbol design in (9), aside from the new scale factor beta, combined with the decorrelating filter of (28) was derived in [9]. Here we examine the processing gain that results from using the DP (9), SDP (13), and SWF (18) symbol design methods in conjunction with three prospective filtering schemes. Recall that for the extreme case of  $m = 0$ , the DP method provides the processing gain for the DSSS method. Similarly, for  $m = NM$  the SWF design method has the same processing gain as the WF symbol design of (15). The filter structures examined here are the matched filter, the decorrelating filter, and a modification to the diagonally-loaded decorrelating filter.

While each filter will be explored in conjunction with the symbol design methods, the general definitions are given here. The familiar matched filter is defined as

$$\mathbf{w}_{\text{MF},k} = \mathbf{c}_k, \quad (30)$$

and the decorrelating filter structure is

$$\begin{aligned} \mathbf{w}_{\text{DF},k} &= (\mathbf{S}\mathbf{S}^H)^{-1} \mathbf{c}_k \\ &= \mathbf{V}\mathbf{\Lambda}^{-1}\mathbf{V}^H \mathbf{c}_k. \end{aligned} \quad (31)$$

Assuming the receiver can determine the clutter and noise power, we also consider a different loaded decorrelating filter useful for analysis purposes, which is defined as

$$\mathbf{w}_{\text{LDF},k} = \mathbf{V}\tilde{\mathbf{\Lambda}}^{-1}\mathbf{V}^H \mathbf{c}_k, \quad (32)$$

where the modified eigenvalue matrix is

$$\tilde{\mathbf{\Lambda}} = \sigma_x^2 \mathbf{\Lambda} + \sigma_u^2 \mathbf{I}. \quad (33)$$

The incident SINR at the receiver can be found via examination of the squared magnitude of the received signal  $\|\mathbf{y}\|^2$ , where the dependence on  $\ell$  is excluded for brevity. The expectation of the squared magnitude of the received signal when a symbol is present is [9]

$$\begin{aligned} E[\|\mathbf{y}\|^2] &= E[(\mathbf{S}\mathbf{x} + \alpha\mathbf{c}_k + \mathbf{u})^H (\mathbf{S}\mathbf{x} + \alpha\mathbf{c}_k + \mathbf{u})] \\ &= E[(\mathbf{S}\mathbf{x})^H (\mathbf{S}\mathbf{x})] + E[(\alpha\mathbf{c}_k)^H (\alpha\mathbf{c}_k)] + E[\mathbf{u}^H \mathbf{u}] \\ &= R_i + S_i + N_i \end{aligned} \quad (34)$$

assuming the noise and clutter process are zero-mean and uncorrelated, and where  $\alpha$  subsumes transmit gain and propagation path loss. The term  $R_i$  represents the incident clutter power,  $S_i$  is the incident signal power, and  $N_i$  is the incident noise power. All symbol design methods included a scaling term, resulting in

$$S_i = |\alpha|^2 \quad (35)$$

while the interference power and noise power are given as

$$\begin{aligned} R_i &= \sigma_x^2 \text{tr}\{\mathbf{\Lambda}\} \\ &= \sigma_x^2 NM \end{aligned} \quad (36)$$

and

$$N_i = \sigma_u^2 NM, \quad (37)$$

respectively. Thus in general the incident (input) SINR is

$$\text{SINR}_i = \frac{|\alpha|^2}{NM(\sigma_x^2 + \sigma_u^2)}. \quad (38)$$

For an arbitrary filter  $\mathbf{w}_k$  the output SINR is found from the expression

$$\begin{aligned} E[|\mathbf{w}_k^H \mathbf{y}|^2] &= E[(\mathbf{S}\mathbf{x} + \alpha\mathbf{c}_k + \mathbf{u})^H \mathbf{w}_k \mathbf{w}_k^H (\mathbf{S}\mathbf{x} + \alpha\mathbf{c}_k + \mathbf{u})] \\ &= E[(\mathbf{S}\mathbf{x})^H \mathbf{w}_k \mathbf{w}_k^H (\mathbf{S}\mathbf{x})] + E[(\alpha\mathbf{c}_k)^H \mathbf{w}_k \mathbf{w}_k^H (\alpha\mathbf{c}_k)] \\ &\quad + E[\mathbf{u}^H \mathbf{w}_k \mathbf{w}_k^H \mathbf{u}] \\ &= R_o + S_o + N_o. \end{aligned} \quad (39)$$

The combination of symbol structure and receive filter determine the processing gain of the receiver. The output SINR is defined as

$$\text{SINR}_o = \frac{S_o}{R_o + N_o} \quad (40)$$

where the clutter power after filtering is, from (39),

$$\begin{aligned}
R_o &= E \left[ (\mathbf{S}\mathbf{x})^H \mathbf{w}_k \mathbf{w}_k^H (\mathbf{S}\mathbf{x}) \right] \\
&= E \left[ \mathbf{w}_k^H \mathbf{S} \mathbf{x} \mathbf{x}^H \mathbf{S}^H \mathbf{w}_k \right] \\
&= \mathbf{w}_k^H \mathbf{S} E \left[ \mathbf{x} \mathbf{x}^H \right] \mathbf{S}^H \mathbf{w}_k \\
&= \sigma_x^2 \mathbf{w}_k^H \mathbf{S} \mathbf{S}^H \mathbf{w}_k \\
&= \sigma_x^2 \mathbf{w}_k^H \mathbf{V} \mathbf{\Lambda} \mathbf{V}^H \mathbf{w}_k
\end{aligned} \tag{41}$$

and the noise power after filtering is similarly found to be

$$\begin{aligned}
N_o &= E \left[ \mathbf{u}^H \mathbf{w}_k \mathbf{w}_k^H \mathbf{u} \right] \\
&= E \left[ \text{tr} \left\{ \mathbf{w}_k^H \mathbf{u} \mathbf{u}^H \mathbf{w}_k \right\} \right] \\
&= \text{tr} \left\{ \mathbf{w}_k^H E \left[ \mathbf{u} \mathbf{u}^H \right] \mathbf{w}_k \right\} \\
&= \sigma_u^2 \mathbf{w}_k^H \mathbf{w}_k.
\end{aligned} \tag{42}$$

The signal power must be determined separately for each symbol type. The processing gain for each symbol design/filter structure is derived in Appendix A

#### A. Processing Gain Comparison

Let us now examine the processing gains afforded by the various combinations of symbol design and filter combinations. As was the case in Section II-E, the radar waveform is an LFM chirp with time-bandwidth product  $N = 64$  with an oversampling factor (relative to the 3 dB bandwidth) of  $M = 2$ . We consider two scenarios. First is the typical case of high clutter-to-noise ratio (CNR), here set to 30 dB. Second, we consider the case of a CNR = 0 dB, where the clutter power is equal to the noise power. As the symbol designs and filters are constructed to take advantage of the masking interference provided by the radar clutter, a CNR of 0 dB provides a "worst case" scenario of the processing gain for each symbol/filter combination.

For the baseline case of DSSS symbol generation, the MF produces a gain equal to the time-bandwidth product of the symbol (which is  $2 \times 64 = 128$ , or 21.1 dB). For a CNR of 30 dB, LDF and DF filtering of the DSSS symbol both produce a processing gain of 35.74 dB by virtue of clutter cancellation. Alternatively, for a CNR of 0 dB, the LDF filter provides a processing gain of 22.2 dB and the DF filter provides a processing gain of 19.4 dB. Therefore, for both

high and low CNRs the LDF provides an advantage over the MF and DF if the clutter and noise powers are accurately estimated.

Figures 7-9 show the processing gains for the DP, SDP, and SWF symbol designs for each of the three filter structures. The high CNR ( $= 30$  dB) case is denoted by solid lines, while the low CNR ( $= 0$  dB) case is shown with dotted lines. For the high CNR case, the clutter degrades MF performance. However, at low CNR the MF is comparable to the DF and LDF filter structures. Comparing Figures 7 and 8, when DP symbols are used in conjunction with the DF or LDF filters the processing gain is less sensitive to the size of the dominant subspace than when the SDP symbols are used.

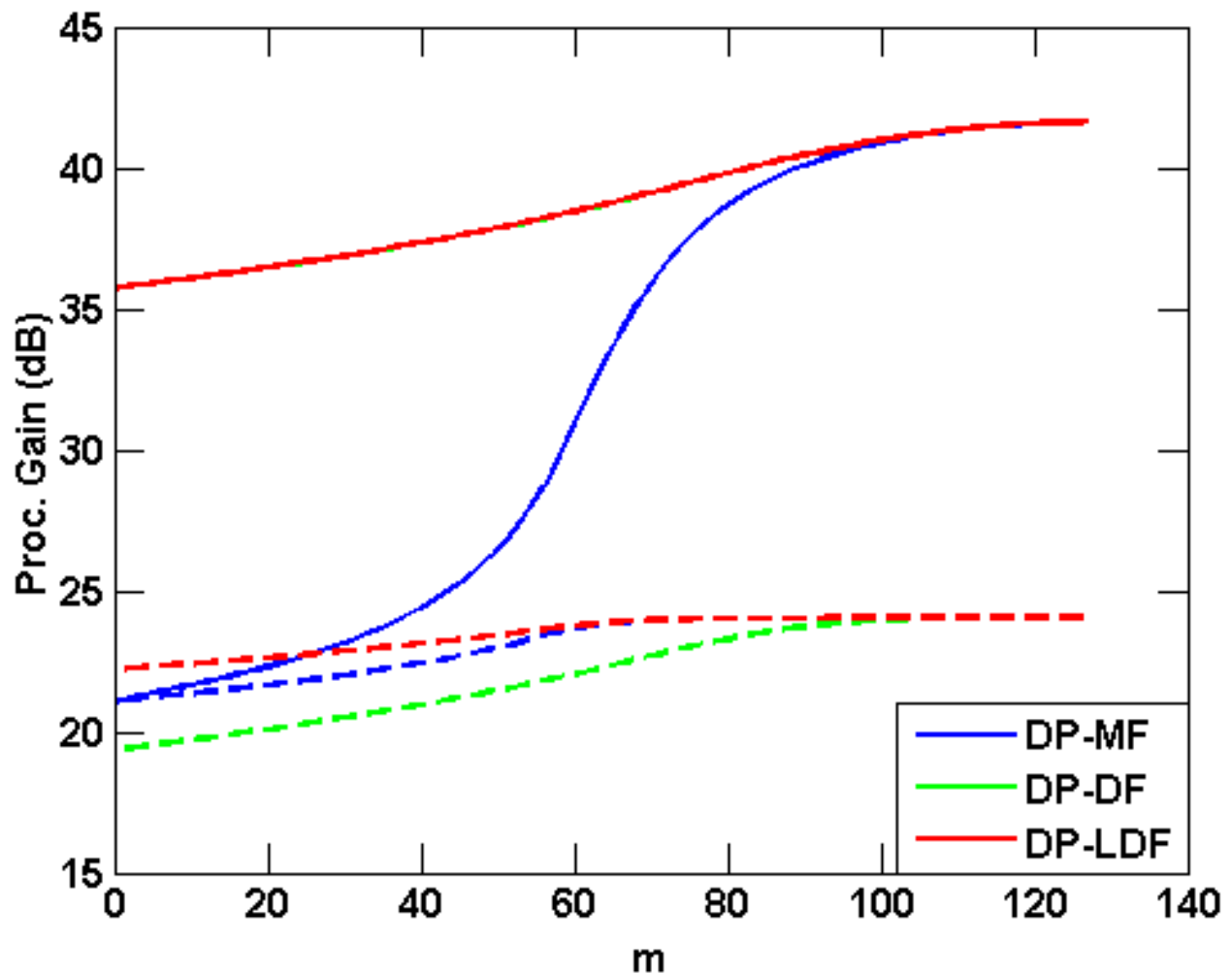


Fig. 7: Analytical processing gain for DP symbol for different receive filters, with high CNR (solid) and low CNR (dashed)

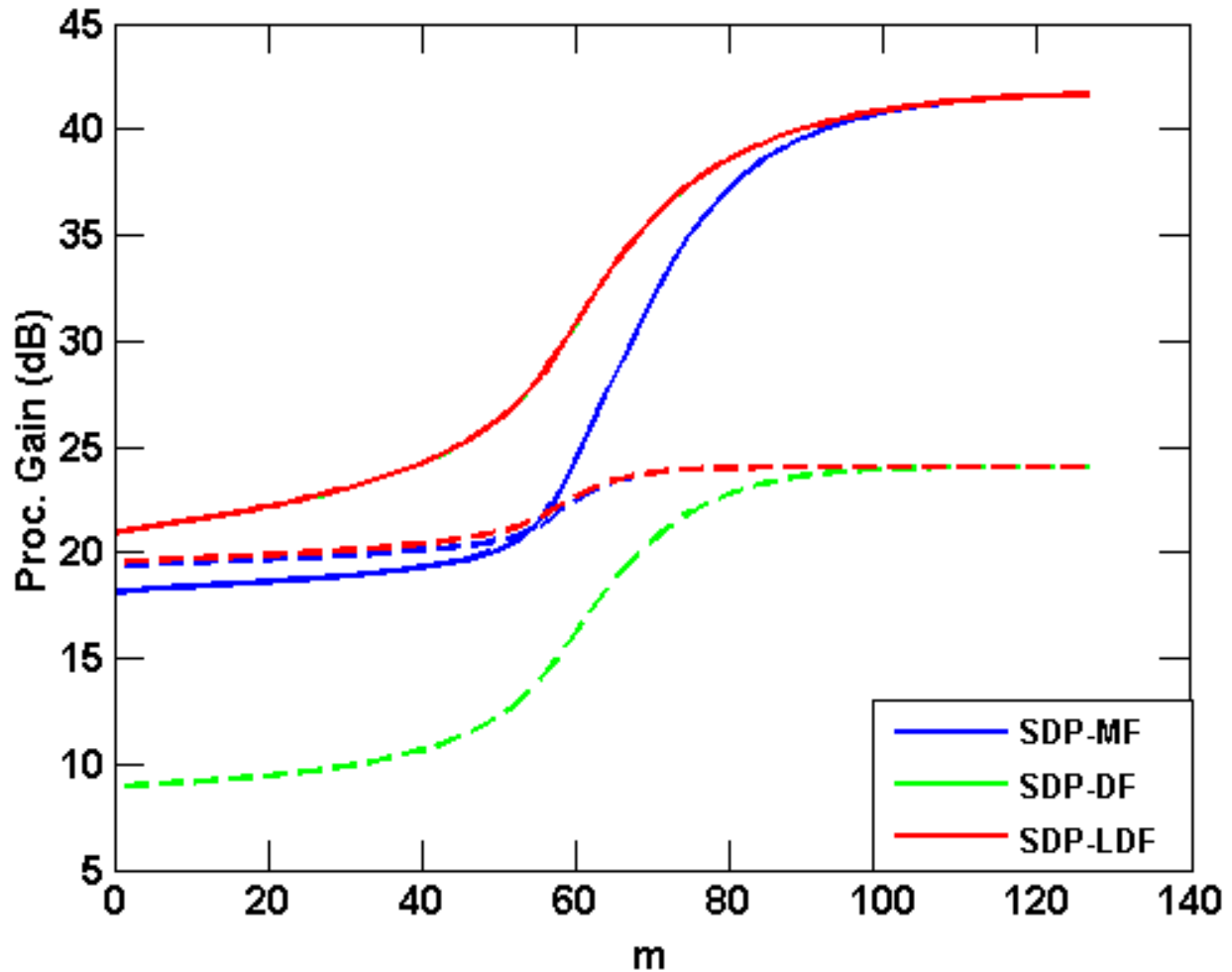


Fig. 8: Analytical processing gain for SDP symbol for different receive filters, with high CNR (solid) and low CNR (dashed)

Figure 9 gives the processing gains for the SWF symbols when the MF, DF, and LDF filters are used. For the high CNR case, the DF and LDF are comparable, and provide superior gain when compared to the MF. However, for the low CNR case, filtering with the MF and DF yields processing gain values that approach the coherent processing gain. However, the LDF is largely unaffected whether the CNR is high or low. Therefore, the LDF is the best filter design to use in conjunction with the SWF symbol.

Figure 10 compares the processing gain of the three proposed symbol design methods at a CNR of 30 dB. The SDP and SWF symbols are filtered with the LDF, while due to the behavior at high values of  $m$  we filter the DP symbol with the DF. Note that the DP symbol offers a higher

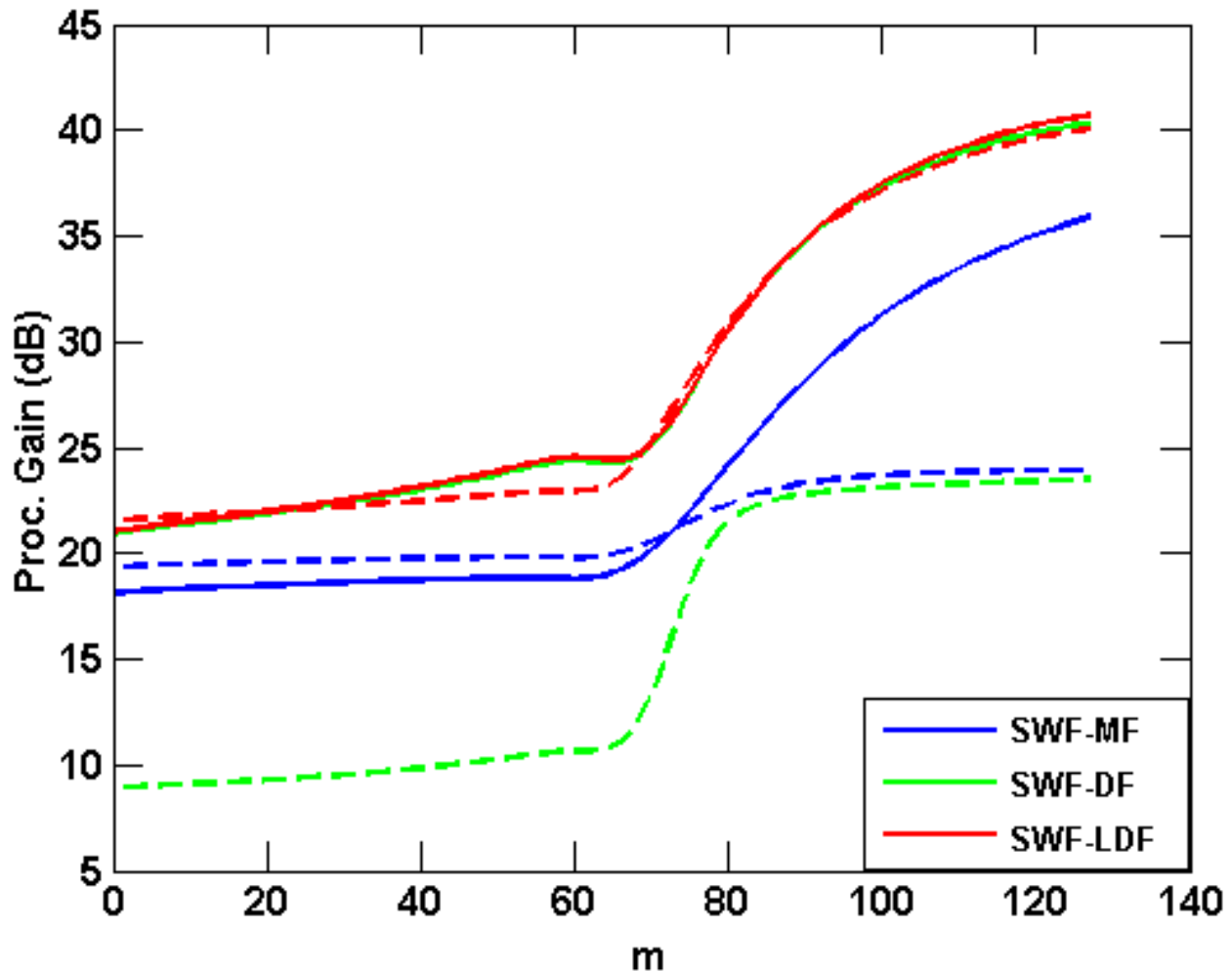


Fig. 9: Analytical processing gain for SWF symbol for different receive filters, with high CNR (solid) and low CNR (dashed)

processing gain than the DSSS symbol at all values of  $m$ , while the SDP and SWF symbols only enjoy a higher processing gain for large values of  $m$ .

Figure 11 compares the processing gain for a CNR of 0 dB. In this case the DP and SDP methods enjoy  $\approx 3$  dB gain advantage over the traditional DSSS method. However, as was shown in Figure 9, the processing gain is largely unaffected by the clutter power when the SWF symbol is used in conjunction with the LDF filter.

## V. INTERCEPT AND DETECTION EVALUATION

Section IV-A compared the processing gain afforded by the various combinations of symbol designs and filter structures. Here, Monte Carlo simulations are used to examine the probabilities

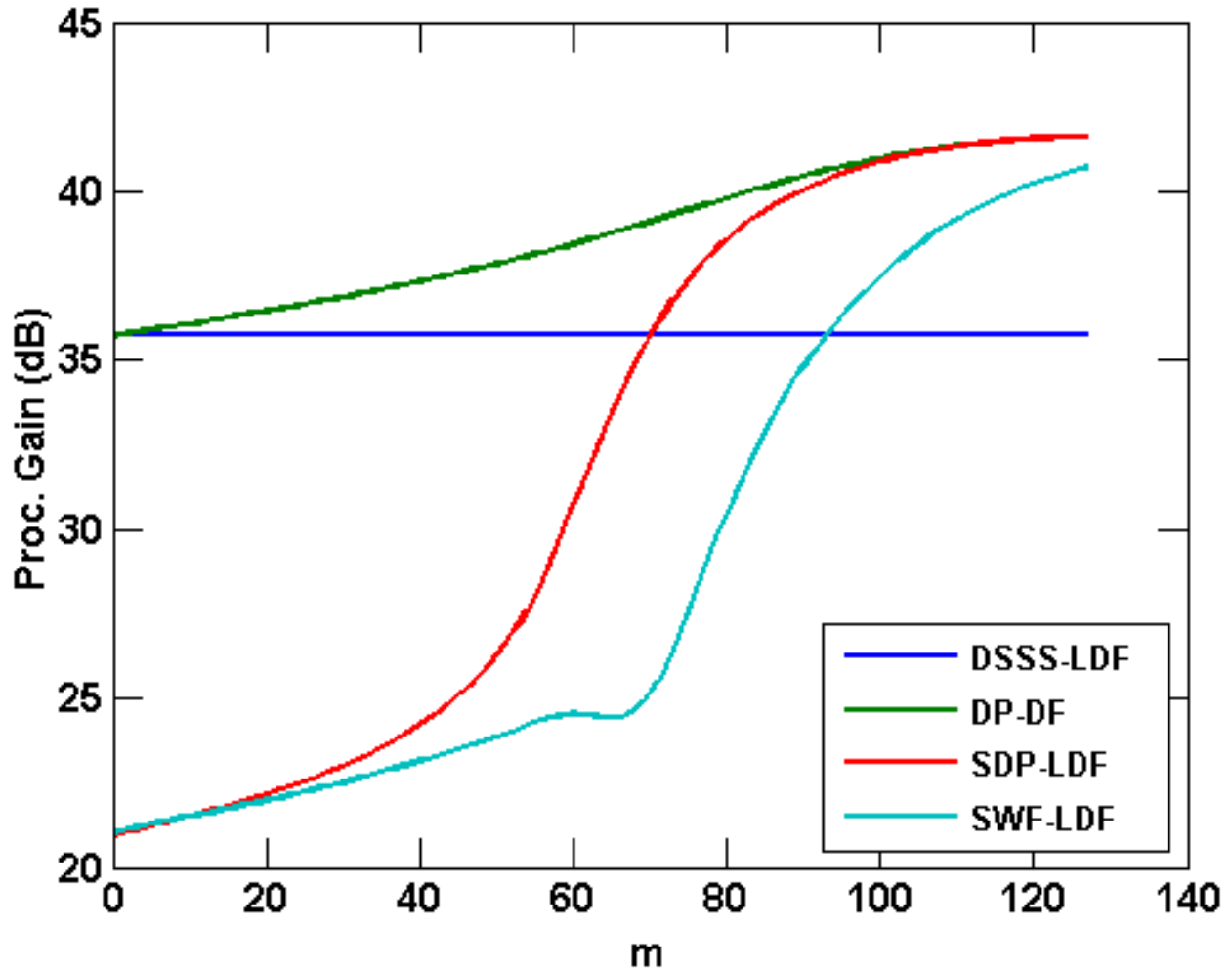


Fig. 10: Comparison of processing gains for high CNR condition

of detection and intercept. In particular, we establish the ability of the two-stage NP receiver of Figure 6 to asynchronously detect the correct transmitted symbol and compare it to the capability of an intercept receiver to detect whether a symbol is present.

#### A. Intercept Receiver

Where Figure 10 shows the high processing gain of the SDP and DP symbols when the size of the non-dominant subspace is small ( $m$  large), Figure 4 shows that the resulting spectral response of such symbols is high where the masking clutter is low. Thus the possible processing gain enhancement for a particular symbol design must be tempered by the associated LPI nature that it represents. To examine the LPI property we use the intercept metric proposed in [9],

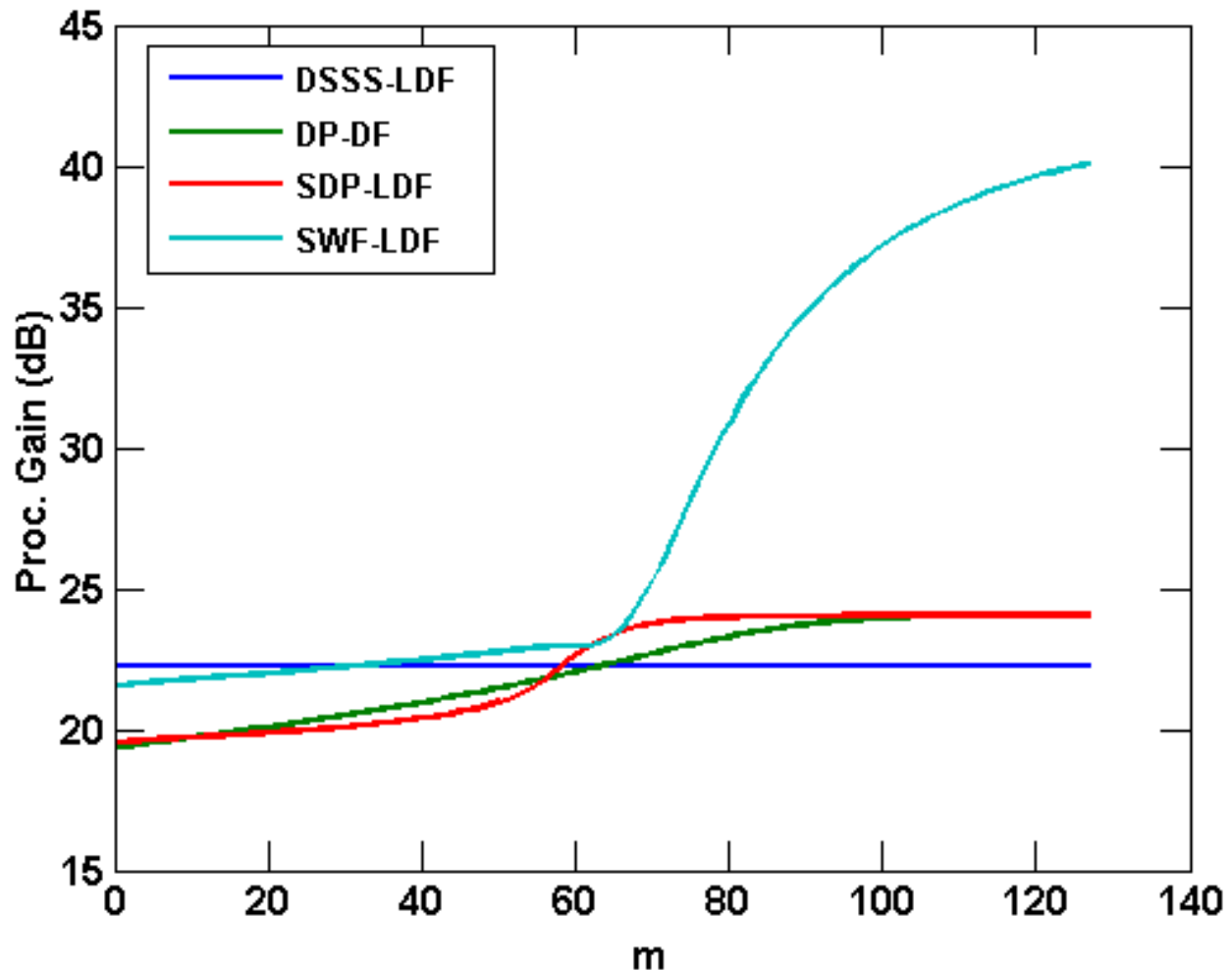


Fig. 11: Comparison of processing gains for low CNR condition

defined as

$$\epsilon(\tilde{m}) = \mathbf{y}^H \mathbf{P}_{\tilde{m}} \mathbf{y} \quad (43)$$

where the projection matrix  $\mathbf{P}_{\tilde{m}}$  is

$$\mathbf{P}_{\tilde{m}} = \mathbf{V}_{\text{ND},\tilde{m}} \mathbf{V}_{\text{ND},\tilde{m}}^H \quad (44)$$

for  $\tilde{m} \in [0, NM]$ .

In other words, the intercept receiver progressively projects out the dominant subspace and then performs energy detection. The full space (*i.e.*  $\tilde{m} = 0$ ) response of (43) coincides with the classic total power radiometer (TPR) [11]. When the intercept receiver projects out the 3 dB bandwidth of the radar waveform (*i.e.*  $\tilde{m} = N$ ), (43) is a subspace implementation of the interference nulling detector of [11].

To provide a "worst case" assessment from a covert communication system perspective, we assume that the intercept receiver possesses knowledge of several transmission parameters that would not necessarily be available to it in practice. Namely, the intercept receiver knows the oversampling factor  $M$  and the time-bandwidth product  $N$ . In addition, we assume that the intercept receiver knows the size of the dominant subspace (*i.e.*  $\tilde{m} = m$ ) and has clairvoyant knowledge of the proper detection threshold to maintain the desired false alarm rate.

### B. Probability of Detection Analysis

We again consider an LFM radar waveform with a time-bandwidth of  $N = 64$  that is oversampled by a factor of  $M = 2$ . A symbol alphabet size of  $K = 8$  was chosen, yielding  $\log_2(K) = 3$  bits/symbol. To provide a high fidelity estimate, the communication symbols are up-sampled by a factor of 4 to simulate the continuous transmission of a communication waveform. All clutter and noise is added at this "continuous" stage and the signal-to-noise ratio (SNR) and clutter-to-noise ratio (CNR) are set in the continuous domain. The CNR is 30 dB for all cases. The resultant symbols are decimated by 4 to provide a "sampled" discrete input to the two-stage NP receiver and intercept receiver. In all cases, the NP receiver and intercept receiver maintain a  $P_{fa} = 10^{-5}$ . Both the desired and intercept receivers scan over an observation interval of  $L = 3NM$  samples to determine if a symbol is present. To provide a metric of LPI performance, we consider the difference in SNR required for successful detection of a symbol by the NP receiver compared to the partially clairvoyant intercept receiver. This difference in SNR required for successful detection is the gain advantage of the desired receiver.

Figure 12 illustrates the probability of detection for a DSSS symbol. The desired receiver uses an LDF filter. We compare three different intercept receiver parameterizations of  $\tilde{m} = 0, 64$ , and 96. The cases of  $\tilde{m} = 0$  and  $\tilde{m} = N = 64$  correspond to the total power radiometer (TPR) and interference canceling receivers of [11], respectively. However, in [11] the interference source occupies a relatively narrow bandwidth with respect to the transmitted symbol. As was shown in Figures 2-4, the clutter response possesses a large spectral rolloff, which helps to mask the communication symbol when  $\tilde{m} = N$ . Therefore, the  $\tilde{m} = 96$  case is included which eliminates most of the clutter response while still leaving a significant portion ( $\approx 25\%$ ) of the symbol power. Figure 12 illustrates the decrease in LPI performance when the intercept receiver eliminates increasing amounts of the clutter. However, the desired receiver still maintains a gain advantage of  $\approx 6$  dB over the intercept receiver, even when the majority of the clutter is canceled.

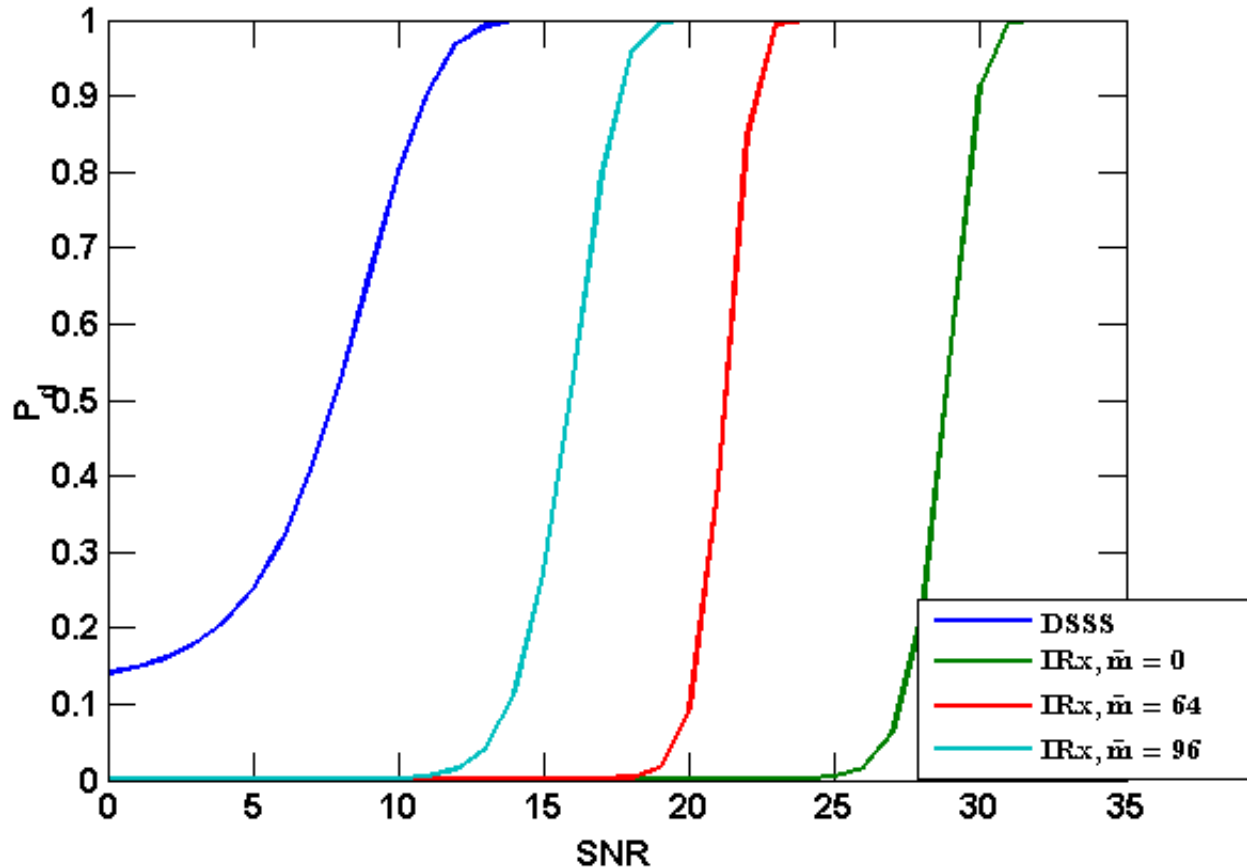


Fig. 12: Probability of detection and intercept for DSSS symbol (i.e. not using masking radar clutter)

Figure 13 verifies the relatively low amount of processing gain variance (as a function of  $m$ ) for the DP symbol/DF filter combination that was observed in Fig. 7. However, note that while transmitting in a portion of the clutter subspace degrades detection performance, it greatly affects intercept performance. The desired receiver enjoys an  $\approx 4$  dB advantage over the intercept receiver when  $m = 96$  versus an  $\approx 17$  dB advantage when  $m = 32$ .

The heavy dependence of processing gain on  $m$  for the SDP symbol is shown in Figure 14, where the desired receiver uses an LDF filter. For the SDP symbol design the choice of  $m = 64$  yields the largest gain advantage for the desired receiver. The spectral shaping of the SDP symbol at  $m = 64$  (as was illustrated in Figure 3) only reduces intercept performance by  $\approx 1$  dB in relation to the DP symbol. Further, the lower processing gain at the same value of  $m$  reduces the detection probability at the desired receiver. Therefore, the increased processing gain afforded by the DP symbol design outweighs the smaller LPI advantage of the SDP symbol

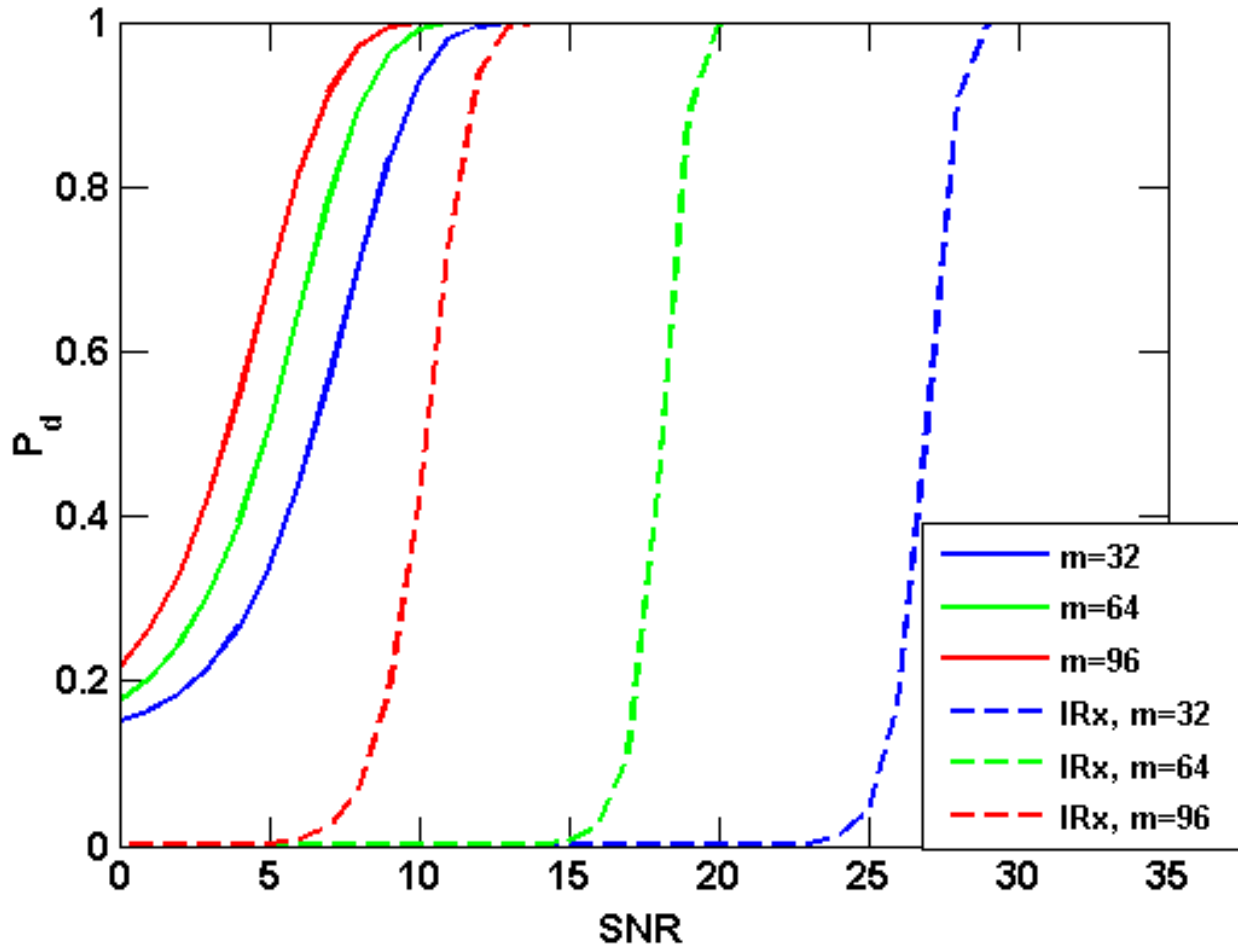


Fig. 13: Probability of detection and intercept for DP symbol

design meaning that spectral shaping alone does not appear to be beneficial.

Figure 15 illustrates the detection characteristics of the SWF symbol design when the desired receiver uses the LDF filter. The similarities between the SDP and SWF symbols at  $m = 32$  and  $m = 64$  (as shown in Figures 2 and 3) carry through to the probability of detection analysis in Figures 14 and 15. However, when  $m = 96$  the SWF symbol deviates significantly from the DP and SDP symbols. Recall from Figure 4 that the SWF symbol at  $m = 96$  allocates reduced power in the clutter subspace (relative to the DSSS symbol), but does not null the clutter subspace like the DP and SDP symbols. The majority of the transmit power allocation occurs in the rolloff region, and significantly less ( $\approx -10$  dB with respect to the DSSS symbol,  $\approx -16$  dB with respect to the DP/SDP symbols) transmit power is allocated at the outer edges of the noise subspace. This behavior allows for  $\approx 14$  dB of gain advantage for the desired receiver, while

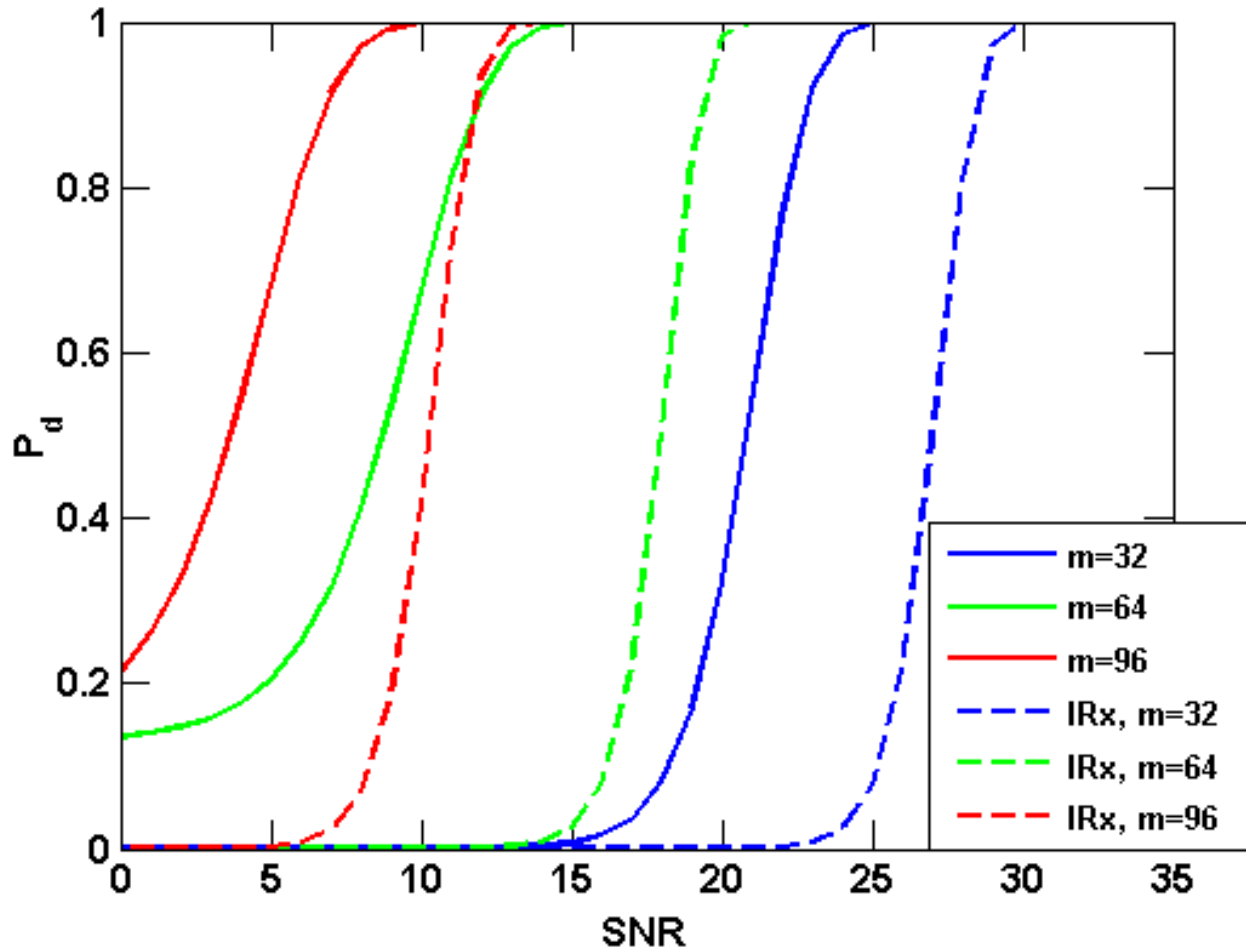


Fig. 14: Probability of detection and intercept for SDP symbol

maintaining the large amount of processing gain shown in Figure 9. As such, one can infer that a judicious spectral distribution of symbol power is one that properly balances between interference avoidance to maximize probability of detection (such as waterfilling provides) and maintaining interference similarity for low probability of intercept.

Finally, in Figure 16 we examine the bit error rates (BER) for the best performing symbol design/filter combinations (with respect to the gain advantage). When the DP symbol is transmitted the desired receiver uses the DF, while the LDF is used when the DSSS, SDP, or SWF symbol is transmitted. In particular, note that the SWF symbol design provides  $\approx 2$ -3 dB of gain over the DP method for a similar BER. Both the SWF and DP symbol designs provide substantial LPI improvements over the DSSS method of symbol design, as well as requiring less power to achieve the same BER.

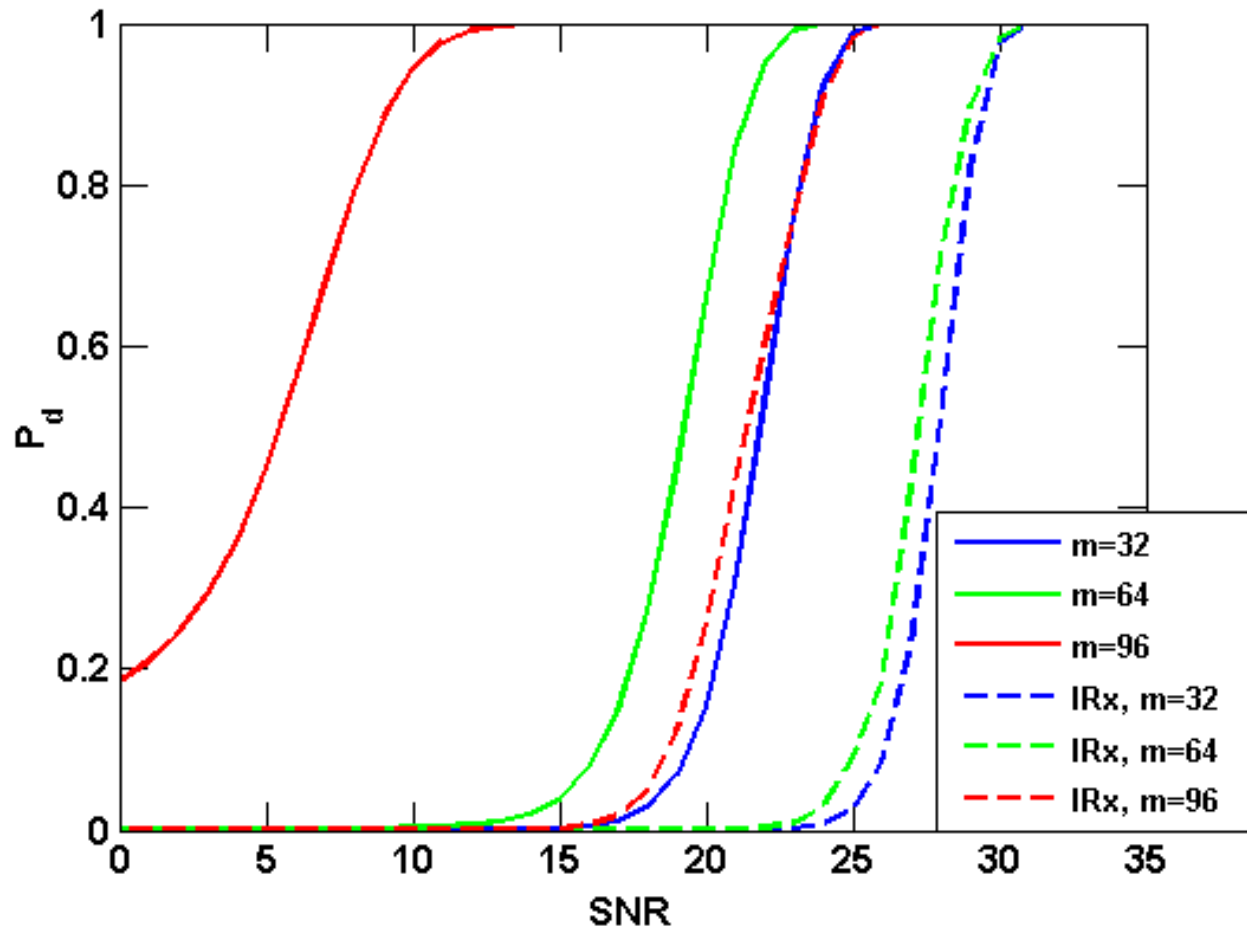


Fig. 15: Probability of detection and intercept for SWF symbol

## VI. CONCLUSION

Several subspace-based symbol design strategies have been presented and examined for LPI communication in the presence of high-power radar emissions. Such subspace strategies are inherently insensitive to timing differences and multipath. Here the previous subspace symbol design methodology was extended to include spectral information in two separate ways: via spectral shaping according to the radar-induced clutter response and using the well-known principle of waterfilling. The purpose for considering these new symbol structures is to ascertain beneficial symbol attributes that much balance between good communication performance and low intercept probability within a litany of practical constraints.

Using multiple receive filtering structures, each of the proposed symbol designs was analytically evaluated in terms of processing gain relative to the masking radar interference. Further,

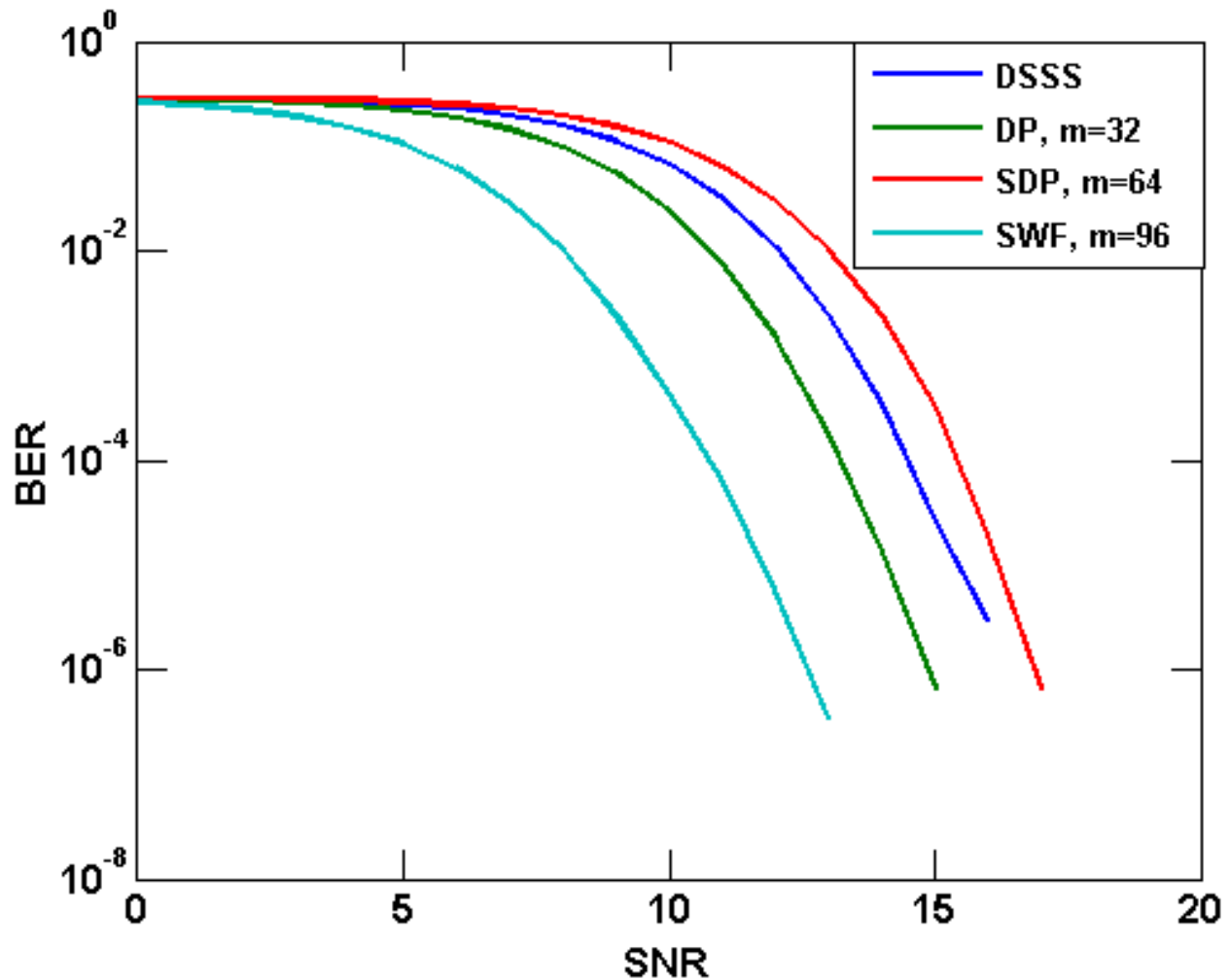


Fig. 16: BER comparison for notable symbol/filter combinations

based on the use of a presumed "worst case" partially clairvoyant intercept receiver, the gain advantage of each symbol design was evaluated. This analysis shows that a hybrid combination of waterfilling and spectral shaping (according to the roll-off region) provides a good compromise between interference avoidance and maintaining interference similarity that should inform the subsequent design of robust optimal symbols.

#### REFERENCES

- [1] V. Winkler, J. Detlefsen, U. Siart, J. Buchler, and M. Wagner, "Automotive radar sensor with communication capability," in *Wireless Technology, 2004. 7th European Conference on*, Oct 2004, pp. 305–308.
- [2] V. Winkler and J. Detlefsen, "Automotive 24 ghz pulse radar extended by a DQPSK communication channel," in *Radar Conference, 2007. EuRAD 2007. European*, Oct 2007, pp. 138–141.

- [3] M. Bocquet, C. Loyez, C. Lethien, N. Deparis, M. Heddebaut, A. Rivenq, and N. Rolland, "A multifunctional 60-ghz system for automotive applications with communication and positioning abilities based on time reversal," in *Radar Conference (EuRAD), 2010 European*, Sept 2010, pp. 61–64.
- [4] L. Reichardt, C. Sturm, F. Grunhaupt, and T. Zwick, "Demonstrating the use of the IEEE 802.11P Car-to-Car communication standard for automotive radar," in *Antennas and Propagation (EUCAP), 2012 6th European Conference on*, March 2012, pp. 1576–1580.
- [5] Shared spectrum access for radar and communications (SSPARC). [Online]. Available: [http://www.darpa.mil/Our\\_Work/STO/Programs/Shared\\_Spectrum\\_Access\\_for\\_Radar\\_and\\_Communications\\_\(SSPARC\).aspx](http://www.darpa.mil/Our_Work/STO/Programs/Shared_Spectrum_Access_for_Radar_and_Communications_(SSPARC).aspx)
- [6] S. Blunt and P. Yatham, "Waveform design for radar-embedded communications," in *Waveform Diversity and Design Conference, 2007. International*, June 2007, pp. 214–218.
- [7] S. D. Blunt, P. Yatham, and J. Stiles, "Intrapulse radar-embedded communications," *Aerospace and Electronic Systems, IEEE Transactions on*, vol. 46, no. 3, pp. 1185 –1200, Jul. 2010.
- [8] J. Metcalf, S. Blunt, and E. Perrins, "Detector design and intercept metrics for intra-pulse radar-embedded communications," in *MILITARY COMMUNICATIONS CONFERENCE, 2011 - MILCOM 2011*, 2011, pp. 188–192.
- [9] S. D. Blunt, J. Metcalf, C. Biggs, and E. Perrins, "Performance characteristics and metrics for intra-pulse radar-embedded communications," *Journal of Selected Areas of Communications*, Dec. 2011.
- [10] R. Scholtz, "The origins of spread-spectrum communications," *Communications, IEEE Transactions on*, vol. 30, no. 5, pp. 822 – 854, may 1982.
- [11] J. Gevargiz, P. Das, and L. Milstein, "Adaptive narrow-band interference rejection in a DS spread-spectrum intercept receiver using transform domain signal processing techniques," *Communications, IEEE Transactions on*, vol. 37, no. 12, pp. 1359–1366, 1989.
- [12] C. Fancey and C. Alabaster, "The metrication of low probability of intercept waveforms," in *Waveform Diversity and Design Conference (WDD), 2010 International*, Aug 2010, pp. 000 058–000 062.
- [13] J. Proakis and M. Salehi, *Digital Communications*. McGraw-Hill, 2007.
- [14] B. Lewis and F. Kretschmer, "Linear frequency modulation derived polyphase pulse compression codes," *Aerospace and Electronic Systems, IEEE Transactions on*, vol. AES-18, no. 5, pp. 637 –641, Sep. 1982.
- [15] S. M. Kay, *Fundamentals of Statistical Signal Processing: Detection Theory*. Prentice Hall PTR, 1998.
- [16] J. Sijbers, A. den Dekker, E. Raman, and D. Van Dyck, "Parameter estimation from magnitude MR images," *International Journal of Imaging Systems and Technology*, vol. 10, pp. 109–114, 1999.
- [17] S. Verdu, *Multiuser Detection*. Cambridge University Press, 2003.
- [18] R. Lupas and S. Verdu, "Linear multiuser detectors for synchronous code-division multiple-access channels," *Information Theory, IEEE Transactions on*, vol. 35, no. 1, pp. 123–136, 1989.

## APPENDIX A

### PROCESSING GAIN DERIVATIONS

The processing gain for the three symbol design methods is derived here for each of the filter structures under consideration.

### A. Processing Gain of Dominant Projection (DP) Symbols

When the DP symbol design of (9) is used in conjunction with a matched filter, the output symbol power is found from (11) and (39) as

$$\begin{aligned} S_{o,DP-MF} &= |\alpha|^2 |\mathbf{w}_{DP-MF,k}^H \mathbf{c}_{DP,k}|^2 \\ &= |\alpha|^2 |\mathbf{c}_{DP,k}^H \mathbf{c}_{DP,k}|^2 = |\alpha|^2 \end{aligned} \quad (45)$$

and the filtered interference and noise powers are found from (9), (10), (41), and (42) to be

$$\begin{aligned} R_{o,DP-MF} &= \sigma_x^2 \mathbf{w}_{DP-MF,k}^H \mathbf{V} \mathbf{\Lambda} \mathbf{V}^H \mathbf{w}_{DP-MF,k} \\ &= \sigma_x^2 \beta_{DP,m} \mathbf{q}_{ND,k}^H \mathbf{V}_{ND,m}^H \mathbf{V} \mathbf{\Lambda} \mathbf{V}^H \mathbf{V}_{ND,m} \mathbf{q}_{ND,k} \\ &\approx \sigma_x^2 \frac{\text{tr}\{\mathbf{\Lambda}_{ND,m}\}}{NM-m}, \end{aligned} \quad (46)$$

and

$$\begin{aligned} N_{o,DP-MF} &= \sigma_u^2 \mathbf{w}_{DP-MF,k}^H \mathbf{w}_{DP-MF,k} \\ &= \sigma_u^2 \beta_{DP,m} \mathbf{q}_{ND,k}^H \mathbf{V}_{ND,m}^H \mathbf{V}_{ND,m} \mathbf{q}_{ND,k} \\ &\approx \sigma_u^2 \end{aligned} \quad (47)$$

respectively. Substituting (45)-(47) into (40), the output SINR when a DP symbol is filtered through a matched filter is

$$\text{SINR}_{o,DP-MF}(m) = \frac{|\alpha|^2}{\sigma_x^2 \frac{\text{tr}\{\mathbf{\Lambda}_{ND,m}\}}{NM-m} + \sigma_u^2}. \quad (48)$$

Therefore, from (38) and (48), the processing gain afforded by matched filtering DP symbols is

$$\Delta_{DP-MF}(m) = \frac{NM(\sigma_x^2 + \sigma_u^2)}{\sigma_x^2 \frac{\text{tr}\{\mathbf{\Lambda}_{ND,m}\}}{NM-m} + \sigma_u^2}. \quad (49)$$

Substituting (9) into (31), the decorrelating filter for a DP symbol takes the form

$$\begin{aligned} \mathbf{w}_{DP-MF,k} &= \mathbf{V} \mathbf{\Lambda}^{-1} \mathbf{V}^H \left( \beta_{DP,m}^{1/2} \mathbf{V}_{ND,m} \mathbf{q}_{ND,k} \right) \\ &= \beta_{DP,m}^{1/2} \mathbf{V} \begin{bmatrix} \mathbf{0}_{m \times (NM-m)} \\ \mathbf{\Lambda}_{ND}^{-1} \end{bmatrix} \mathbf{q}_{ND,k}. \end{aligned} \quad (50)$$

The signal power after processing a DP symbol with the filter of (50) is found from (9) and (12) as

$$\begin{aligned}
S_{o,DP-DF} &= |\alpha|^2 |\mathbf{w}_{DP-DF,k}^H \mathbf{c}_{DP,k}|^2 \\
&= |\alpha|^2 \left| \beta_{DP,m} \mathbf{q}_{ND,k}^H \left[ \mathbf{0}_{(NM-m) \times m} \mid \mathbf{\Lambda}_{ND}^{-1} \right] \mathbf{V}^H \mathbf{V}_{ND,m} \mathbf{q}_{ND,k} \right|^2 \\
&\approx \frac{|\alpha|^2 \beta_{DP,m}^2}{(NM)^2} (\text{tr} \{ \mathbf{\Lambda}_{ND,m}^{-1} \})^2 \\
&= \frac{|\alpha|^2 (\text{tr} \{ \mathbf{\Lambda}_{ND,m}^{-1} \})^2}{(NM - m)^2}.
\end{aligned} \tag{51}$$

The interference power after filtering with the decorrelating filter of (50) is, using (10), (12), and (41),

$$\begin{aligned}
R_{o,DP-DF} &= \sigma_x^2 \mathbf{w}_{DP-DF,k}^H \mathbf{V} \mathbf{\Lambda} \mathbf{V}^H \mathbf{w}_{DP-DF,k} \\
&= \sigma_x^2 \beta_{DP,m} \mathbf{q}_{ND,k}^H \left[ \mathbf{0} \mid \mathbf{\Lambda}_{ND}^{-1} \right] \mathbf{\Lambda} \begin{bmatrix} \mathbf{0} \\ \mathbf{\Lambda}_{ND}^{-1} \end{bmatrix} \mathbf{q}_{ND,k} \\
&\approx \sigma_x^2 \frac{\text{tr} \{ \mathbf{\Lambda}_{ND,m}^{-1} \}}{NM - m},
\end{aligned} \tag{52}$$

and the noise power is, using (10), (12), and (42),

$$\begin{aligned}
N_{o,DP-DF} &= \sigma_u^2 \mathbf{w}_{DP-DF,k}^H \mathbf{w}_{DP-DF,k} \\
&= \sigma_u^2 \beta_{DP,m} \mathbf{q}_{ND,k}^H \left[ \mathbf{0} \mid \mathbf{\Lambda}_{ND}^{-1} \right] \mathbf{V}^H \mathbf{V} \begin{bmatrix} \mathbf{0} \\ \mathbf{\Lambda}_{ND}^{-1} \end{bmatrix} \mathbf{q}_{ND,k} \\
&\approx \sigma_u^2 \frac{\text{tr} \{ \mathbf{\Lambda}_{ND,m}^{-2} \}}{NM - m}.
\end{aligned} \tag{53}$$

Combining the results of (51)-(53) results in the output SINR

$$\begin{aligned}
\text{SINR}_{o,DP-DF}(m) &= \\
&= \frac{|\alpha|^2 (\text{tr} \{ \mathbf{\Lambda}_{ND,m}^{-1} \})^2}{(NM - m) (\sigma_x^2 \text{tr} \{ \mathbf{\Lambda}_{ND,m}^{-1} \} + \sigma_u^2 \text{tr} \{ \mathbf{\Lambda}_{ND,m}^{-2} \})}.
\end{aligned} \tag{54}$$

Relative to (38), the processing gain of the decorrelating filter/dominant projection combination is then

$$\begin{aligned}
\Delta_{DP-DF}(m) &= \\
&= \frac{NM(\sigma_x^2 + \sigma_u^2) (\text{tr} \{ \mathbf{\Lambda}_{ND,m}^{-1} \})^2}{(NM - m) (\sigma_x^2 \text{tr} \{ \mathbf{\Lambda}_{ND,m}^{-1} \} + \sigma_u^2 \text{tr} \{ \mathbf{\Lambda}_{ND,m}^{-2} \})}.
\end{aligned} \tag{55}$$

The third filter structure we consider for the DP symbols is the loaded decorrelating filter of (32). For a DP symbol, (32) becomes

$$\begin{aligned}\mathbf{w}_{\text{DP-LDF},k} &= \mathbf{V}\tilde{\Lambda}^{-1}\mathbf{V}^H \left( \beta_{\text{DP},m}^{1/2} \mathbf{V}_{\text{ND},m} \mathbf{q}_{\text{ND},k} \right) \\ &= \beta_{\text{DP},m}^{1/2} \mathbf{V} \begin{bmatrix} \mathbf{0} \\ \tilde{\Lambda}_{\text{ND}}^{-1} \end{bmatrix} \mathbf{q}_{\text{ND},k}.\end{aligned}\quad (56)$$

Following similar derivations as those in (51)-(53), it can be shown that the a DP symbol filtered through the loaded decorrelating filter of (56) has an expected SINR of

$$\begin{aligned}\text{SINR}_{o,\text{DP-LDF}}(m) &= \\ &= \frac{|\alpha|^2 \left( \text{tr} \left\{ \tilde{\Lambda}_{\text{ND},m}^{-1} \right\} \right)^2}{(NM - m) \left( \sigma_x^2 \text{tr} \left\{ \tilde{\Lambda}_{\text{ND},m}^{-2} \Lambda_{\text{ND},m} \right\} + \sigma_u^2 \text{tr} \left\{ \tilde{\Lambda}_{\text{ND},m}^{-2} \right\} \right)}.\end{aligned}\quad (57)$$

The processing gain of the loaded decorrelating filter is then

$$\begin{aligned}\Delta_{\text{DP-LDF}}(m) &= \\ &= \frac{NM(\sigma_x^2 + \sigma_u^2) \left( \text{tr} \left\{ \tilde{\Lambda}_{\text{ND},m}^{-1} \right\} \right)^2}{(NM - m) \left( \sigma_x^2 \text{tr} \left\{ \tilde{\Lambda}_{\text{ND},m}^{-2} \Lambda_{\text{ND},m} \right\} + \sigma_u^2 \text{tr} \left\{ \tilde{\Lambda}_{\text{ND},m}^{-2} \right\} \right)}.\end{aligned}\quad (58)$$

### B. Processing Gain of Shaped Waterfilling (SWF) Symbols

The second symbol design method under examination is the shaped waterfilling (SWF) method. Like (45), the scaling factor  $\beta_{\text{SWF}}$  causes the output power of a matched filter processing the SWF symbol of (18) to be the magnitude squared of the complex gain coefficient

$$S_{o,\text{SWF-MF}} = |\alpha|^2 |\mathbf{w}_{\text{SWF-MF},k}^H \mathbf{c}_{\text{SWF},k}|^2 = |\alpha|^2. \quad (59)$$

The interference and noise powers after matched filtering with (18) are found from (41) and (42) to be

$$\begin{aligned}R_{o,\text{SWF-MF}} &= \sigma_x^2 \mathbf{w}_{\text{SWF-MF},k}^H \mathbf{V} \Lambda \mathbf{V}^H \mathbf{w}_{\text{SWF-MF},k} \\ &= \sigma_x^2 \beta_{\text{SWF},m} \mathbf{q}_k^H \Lambda_{\text{P},m}^{1/2} \mathbf{V}^H \mathbf{V} \Lambda \mathbf{V}^H \mathbf{V} \Lambda_{\text{P},m}^{1/2} \mathbf{q}_k \\ &\approx \sigma_x^2 \frac{\text{tr} \left\{ \Lambda_{\text{P},m} \Lambda \right\}}{\text{tr} \left\{ \Lambda_{\text{P},m} \right\}} \\ &= \sigma_x^2 \frac{m + \text{tr} \left\{ \Lambda_{\text{ND},m}^2 \right\}}{\text{tr} \left\{ \Lambda_{\text{P},m} \right\}},\end{aligned}\quad (60)$$

and

$$N_{o,\text{SWF-MF}} = \sigma_u^2 \mathbf{w}_{\text{SWF-MF},k}^H \mathbf{w}_{\text{SWF-MF},k} = \sigma_u^2, \quad (61)$$

respectively. Combining (59)-(61), the SINR after processing a SWF symbol with a matched filter is

$$\text{SINR}_{o,\text{SWF-MF}}(m) = \frac{|\alpha|^2}{\sigma_x^2 \frac{m + \text{tr}\{\Lambda_{\text{ND},m}^2\}}{\text{tr}\{\Lambda_{\text{P},m}\}} + \sigma_u^2} \quad (62)$$

so the resultant processing gain is

$$\Delta_{\text{SWF-MF}}(m) = \frac{NM(\sigma_x^2 + \sigma_u^2)}{\sigma_x^2 \frac{m + \text{tr}\{\Lambda_{\text{ND},m}^2\}}{\text{tr}\{\Lambda_{\text{P},m}\}} + \sigma_u^2}. \quad (63)$$

The decorrelating filter corresponding to the SWF symbol is found by applying (18) to (31) as

$$\begin{aligned} \mathbf{w}_{\text{SWF-DF},k} &= \mathbf{V}\Lambda^{-1}\mathbf{V}^H \left( \beta_{\text{SWF},m}^{1/2} \mathbf{V}\Lambda_{\text{P},m}^{1/2} \mathbf{q}_k \right) \\ &= \beta_{\text{SWF},m}^{1/2} \mathbf{V}\Lambda^{-1}\Lambda_{\text{P},m}^{1/2} \mathbf{q}_k. \end{aligned} \quad (64)$$

From (18), filtering an SWF symbol with (64) yields an expected signal power of

$$\begin{aligned} S_{o,\text{SWF-DF}} &= |\alpha|^2 |\mathbf{w}_{\text{SWF-DF},k}^H \mathbf{c}_{\text{SWF},k}|^2 \\ &= |\alpha|^2 \left| \beta_{\text{SWF},m} \mathbf{q}_k^H \Lambda_{\text{P},m}^{1/2} \Lambda^{-1} \mathbf{V}^H \mathbf{V} \Lambda_{\text{P},m}^{1/2} \mathbf{q}_k \right|^2 \\ &\approx \frac{|\alpha|^2 \beta_{\text{SWF},m}^2}{(NM)^2} (\text{tr}\{\Lambda_{\text{P},m} \Lambda^{-1}\})^2 \\ &= \frac{|\alpha|^2 (\text{tr}\{\Lambda_{\text{D}}^{-2}\} + NM - m)^2}{(\text{tr}\{\Lambda_{\text{P},m}\})^2}. \end{aligned} \quad (65)$$

The interference power after processing with the decorrelating filter of (64) is, from (41),

$$\begin{aligned} R_{o,\text{SWF-DF}} &= \sigma_x^2 \mathbf{w}_{\text{SWF-DF},k}^H \mathbf{V}\Lambda\mathbf{V}^H \mathbf{w}_{\text{SWF-DF},k} \\ &= \sigma_x^2 \beta_{\text{SWF},m} \mathbf{q}_k^H \Lambda_{\text{P},m}^{1/2} \Lambda^{-1} \mathbf{V}^H \mathbf{V}\Lambda\mathbf{V}^H \mathbf{V}\Lambda^{-1} \Lambda_{\text{P},m}^{1/2} \mathbf{q}_k \\ &\approx \sigma_x^2 \frac{\text{tr}\{\Lambda_{\text{P},m} \Lambda^{-1}\}}{\text{tr}\{\Lambda_{\text{P},m}\}} \\ &= \sigma_x^2 \frac{\text{tr}\{\Lambda_{\text{D},m}^{-2}\} + NM - m}{\text{tr}\{\Lambda_{\text{P},m}\}}, \end{aligned} \quad (66)$$

and the noise power is

$$\begin{aligned}
N_{o,\text{SWF-DF}} &= \sigma_u^2 \mathbf{w}_{\text{SWF-DF},k}^H \mathbf{w}_{\text{SWF-DF},k} \\
&= \sigma_u^2 \beta_{\text{SWF},m} \mathbf{q}_k^H \mathbf{\Lambda}_{\text{P},m}^{1/2} \mathbf{\Lambda}^{-1} \mathbf{V}^H \mathbf{V} \mathbf{\Lambda}^{-1} \mathbf{\Lambda}_{\text{P},m}^{1/2} \mathbf{q}_k \\
&\approx \sigma_u^2 \frac{\text{tr} \{ \mathbf{\Lambda}_{\text{P},m} \mathbf{\Lambda}^{-2} \}}{\text{tr} \{ \mathbf{\Lambda}_{\text{P},m} \}}.
\end{aligned} \tag{67}$$

The SINR after processing the SWF symbol by the decorrelating filter of (64) is found by combining (65)-(67) as

$$\begin{aligned}
\text{SINR}_{o,\text{SWF-DF}}(m) &= \\
&\frac{|\alpha|^2 \left( \text{tr} \{ \mathbf{\Lambda}_{\text{D}}^{-2} \} + NM - m \right)^2}{\text{tr} \{ \mathbf{\Lambda}_{\text{P},m} \} \left( \sigma_x^2 \left( \text{tr} \{ \mathbf{\Lambda}_{\text{D},m}^{-2} \} + NM - m \right) + \sigma_u^2 \text{tr} \{ \mathbf{\Lambda}_{\text{P},m} \mathbf{\Lambda}^{-2} \} \right)}
\end{aligned} \tag{68}$$

so the resultant processing gain is

$$\begin{aligned}
\Delta_{\text{SWF-DF}}(m) &= \\
&\frac{NM(\sigma_x^2 + \sigma_u^2) \left( \text{tr} \{ \mathbf{\Lambda}_{\text{D}}^{-2} \} + NM - m \right)^2}{\text{tr} \{ \mathbf{\Lambda}_{\text{P},m} \} \left( \sigma_x^2 \left( \text{tr} \{ \mathbf{\Lambda}_{\text{D},m}^{-2} \} + NM - m \right) + \sigma_u^2 \text{tr} \{ \mathbf{\Lambda}_{\text{P},m} \mathbf{\Lambda}^{-2} \} \right)}.
\end{aligned} \tag{69}$$

The loaded decorrelating filter (LDF) structure of (32) when applied to the SWF symbol of (18) takes the form

$$\begin{aligned}
\mathbf{w}_{\text{SWF-LDF},k} &= \mathbf{V} \tilde{\mathbf{\Lambda}}^{-1} \mathbf{V}^H \left( \beta_{\text{SWF},m}^{1/2} \mathbf{V} \mathbf{\Lambda}_{\text{P},m}^{1/2} \mathbf{q}_k \right) \\
&= \beta_{\text{SWF},m}^{1/2} \mathbf{V} \tilde{\mathbf{\Lambda}}^{-1} \mathbf{\Lambda}_{\text{P},m}^{1/2} \mathbf{q}_k.
\end{aligned} \tag{70}$$

The derivation of the SINR after processing with the LDF of (70) closely follows the steps taken in (65)-(67), resulting in an output SINR

$$\begin{aligned}
\text{SINR}_{o,\text{SWF-LDF}}(m) &= \\
&\frac{|\alpha|^2 \left( \text{tr} \{ \mathbf{\Lambda}_{\text{P},m} \tilde{\mathbf{\Lambda}}^{-1} \} \right)^2}{\text{tr} \{ \mathbf{\Lambda}_{\text{P},m} \} \left( \sigma_x^2 \text{tr} \{ \mathbf{\Lambda}_{\text{P},m} \tilde{\mathbf{\Lambda}}^{-2} \mathbf{\Lambda} \} + \sigma_u^2 \text{tr} \{ \mathbf{\Lambda}_{\text{P},m} \tilde{\mathbf{\Lambda}}^{-2} \} \right)}.
\end{aligned} \tag{71}$$

which yields a processing gain of

$$\begin{aligned}
\Delta_{\text{SWF-LDF}}(m) &= \\
&\frac{NM(\sigma_x^2 + \sigma_u^2) \left( \text{tr} \{ \mathbf{\Lambda}_{\text{P},m} \tilde{\mathbf{\Lambda}}^{-1} \} \right)^2}{\text{tr} \{ \mathbf{\Lambda}_{\text{P},m} \} \left( \sigma_x^2 \text{tr} \{ \mathbf{\Lambda}_{\text{P},m} \tilde{\mathbf{\Lambda}}^{-2} \mathbf{\Lambda} \} + \sigma_u^2 \text{tr} \{ \mathbf{\Lambda}_{\text{P},m} \tilde{\mathbf{\Lambda}}^{-2} \} \right)}.
\end{aligned} \tag{72}$$

### C. Processing Gain of Shaped Dominant Projection (SDP) Symbols

The final symbol design method under consideration is the shaped dominant projection (SDP) method given in (13). When a matched filter is used, the scaling factor of (14) again causes the signal power after processing to reduce to

$$S_{o,\text{SDP-MF}} = |\alpha|^2 |\mathbf{w}_{\text{SDP-MF},k}^H \mathbf{c}_{\text{SDP},k}|^2 = |\alpha|^2 \quad (73)$$

and the noise power from (42) to become

$$N_{o,\text{SDP-MF}} = \sigma_u^2 \mathbf{w}_{\text{SDP-MF},k}^H \mathbf{w}_{\text{SDP-MF},k} = \sigma_u^2. \quad (74)$$

The clutter power after filtering with the matched filter of (13) is then found from (41) to be

$$\begin{aligned} R_{o,\text{SDP-MF}} &= \sigma_x^2 \mathbf{w}_{\text{SDP-MF},k}^H \mathbf{V} \mathbf{\Lambda} \mathbf{V}^H \mathbf{w}_{\text{SDP-MF},k} \\ &= \sigma_x^2 \beta_{\text{SDP},m} \mathbf{q}_{\text{ND},k}^H \mathbf{\Lambda}_{\text{ND},m}^2 \mathbf{q}_{\text{ND},k} \\ &\approx \sigma_x^2 \frac{\text{tr} \{ \mathbf{\Lambda}_{\text{ND},m}^2 \}}{\text{tr} \{ \mathbf{\Lambda}_{\text{ND},m} \}}, \end{aligned} \quad (75)$$

yielding an expected output SINR of

$$\text{SINR}_{o,\text{SDP-MF}}(m) = \frac{|\alpha|^2}{\sigma_x^2 \frac{\text{tr} \{ \mathbf{\Lambda}_{\text{ND},m}^2 \}}{\text{tr} \{ \mathbf{\Lambda}_{\text{ND},m} \}} + \sigma_u^2}. \quad (76)$$

From (76), the matched filter produces a processing gain for the SDP symbol of

$$\Delta_{\text{SDP,MF}}(m) = \frac{NM(\sigma_x^2 + \sigma_u^2)}{\sigma_x^2 \frac{\text{tr} \{ \mathbf{\Lambda}_{\text{ND},m}^2 \}}{\text{tr} \{ \mathbf{\Lambda}_{\text{ND},m} \}} + \sigma_u^2}. \quad (77)$$

The decorrelating filter associated with the SDP symbol is found by substituting (13) into (31) as

$$\begin{aligned} \mathbf{w}_{\text{SDP-DF},k} &= \mathbf{V} \mathbf{\Lambda}^{-1} \mathbf{V}^H \left( \beta_{\text{SDP},m}^{1/2} \mathbf{V}_{\text{ND},m} \mathbf{\Lambda}_{\text{ND},m}^{1/2} \mathbf{q}_{\text{ND},k} \right) \\ &= \beta_{\text{SDP},m}^{1/2} \mathbf{V} \begin{bmatrix} \mathbf{0}_{m \times (NM-m)} \\ \mathbf{\Lambda}_{\text{ND}}^{-1/2} \end{bmatrix} \mathbf{q}_{\text{ND},k}. \end{aligned} \quad (78)$$

Using (13) and (78), the signal power after the decorrelating filter is

$$\begin{aligned} S_{o,\text{SDP-DF}} &= |\alpha|^2 |\mathbf{w}_{\text{SDP-DF},k}^H \mathbf{c}_{\text{SDP},k}|^2 \\ &= |\alpha|^2 \left| \beta_{\text{SDP},m} \mathbf{q}_{\text{ND},k}^H \text{tr} \left\{ \mathbf{\Lambda}_{\text{ND},m}^{-1/2} \mathbf{\Lambda}_{\text{ND},m}^{1/2} \right\} \mathbf{q}_{\text{ND},k} \right|^2 \\ &\approx \frac{|\alpha|^2 \beta_{\text{SDP},m}^2 (NM - m)^2}{(NM)^2} \\ &= \frac{|\alpha|^2 (NM - m)^2}{(\text{tr} \{ \mathbf{\Lambda}_{\text{ND},m} \})^2}. \end{aligned} \quad (79)$$

Applying (78) to (41) reveals that the interference power after the decorrelating filter is

$$\begin{aligned}
R_{o,\text{SDP-DF}} &= \sigma_x^2 \mathbf{w}_{\text{SDP-DF},k}^H \mathbf{V} \boldsymbol{\Lambda} \mathbf{V}^H \mathbf{w}_{\text{SDP-DF},k} \\
&= \sigma_x^2 \beta_{\text{SDP},m} \mathbf{q}_{\text{ND},k}^H \left[ \mathbf{0} \mid \boldsymbol{\Lambda}_{\text{ND}}^{-1/2} \right] \boldsymbol{\Lambda} \begin{bmatrix} \mathbf{0} \\ \boldsymbol{\Lambda}_{\text{ND}}^{-1/2} \end{bmatrix} \mathbf{q}_{\text{ND},k} \\
&= \sigma_x^2 \frac{(NM - m)}{\text{tr} \{ \boldsymbol{\Lambda}_{\text{ND},m} \}}.
\end{aligned} \tag{80}$$

Similarly, the noise power after the decorrelating filter of (78) is found from (42) to be

$$\begin{aligned}
N_{o,\text{SDP-DF}} &= \sigma_u^2 \mathbf{w}_{\text{SDP-DF},k}^H \mathbf{w}_{\text{SDP-DF},k} \\
&= \sigma_u^2 \beta_{\text{SDP},m} \mathbf{q}_{\text{ND},k}^H \left[ \mathbf{0} \mid \boldsymbol{\Lambda}_{\text{ND}}^{-1/2} \right] \mathbf{V}^H \mathbf{V} \begin{bmatrix} \mathbf{0} \\ \boldsymbol{\Lambda}_{\text{ND}}^{-1/2} \end{bmatrix} \mathbf{q}_{\text{ND},k} \\
&= \sigma_u^2 \frac{\text{tr} \{ \boldsymbol{\Lambda}_{\text{ND},m}^{-1} \}}{\text{tr} \{ \boldsymbol{\Lambda}_{\text{ND},m} \}}.
\end{aligned} \tag{81}$$

Therefore, the output SINR SDP using the decorrelating filter is found from (79)-(81) to be

$$\begin{aligned}
\text{SINR}_{o,\text{SDP-DF}}(m) &= \\
&= \frac{|\alpha|^2 (NM - m)^2}{\text{tr} \{ \boldsymbol{\Lambda}_{\text{ND},m} \} (\sigma_x^2 (NM - m) + \sigma_u^2 \text{tr} \{ \boldsymbol{\Lambda}_{\text{ND},m}^{-1} \})}.
\end{aligned} \tag{82}$$

The processing gain obtained by the decorrelating filter of (78) is then found from (82) and (38)

$$\begin{aligned}
\Delta_{\text{SDP-DF}}(m) &= \\
&= \frac{NM(\sigma_x^2 + \sigma_u^2)(NM - m)^2}{\text{tr} \{ \boldsymbol{\Lambda}_{\text{ND},m} \} (\sigma_x^2 (NM - m) + \sigma_u^2 \text{tr} \{ \boldsymbol{\Lambda}_{\text{ND},m}^{-1} \})}.
\end{aligned} \tag{83}$$

The final design under consideration is an SDP symbol filtered with the LDF structure of (32). From (13) and (32) this filter takes the form

$$\begin{aligned}
\mathbf{w}_{\text{SDP-LDF},k} &= \mathbf{V} \tilde{\boldsymbol{\Lambda}}^{-1} \mathbf{V}^H \left( \beta_{\text{SDP},m}^{1/2} \mathbf{V}_{\text{ND},m} \boldsymbol{\Lambda}_{\text{ND},m}^{1/2} \mathbf{q}_{\text{ND},k} \right) \\
&= \beta_{\text{SDP},m}^{1/2} \mathbf{V} \begin{bmatrix} \mathbf{0}_{m \times (NM-m)} \\ \tilde{\boldsymbol{\Lambda}}_{\text{ND},m}^{-1} \end{bmatrix} \boldsymbol{\Lambda}_{\text{ND},m}^{1/2} \mathbf{q}_{\text{ND},k}.
\end{aligned} \tag{84}$$

Filtering the SDP symbol of (13) with the LDF of (84) results in an average output signal power of

$$\begin{aligned}
S_{o,\text{SDP-LDF}} &= |\alpha|^2 |\mathbf{w}_{\text{SDP-LDF},k}^H \mathbf{c}_{\text{SDP},k}|^2 \\
&= |\alpha|^2 \left| \beta_{\text{SDP},m} \mathbf{q}_{\text{ND},k}^H \mathbf{\Lambda}_{\text{ND},m}^{1/2} \tilde{\mathbf{\Lambda}}_{\text{ND},m}^{-1} \mathbf{\Lambda}_{\text{ND},m}^{1/2} \mathbf{q}_{\text{ND},k} \right|^2 \\
&\approx \frac{|\alpha|^2 \left( \text{tr} \left\{ \mathbf{\Lambda}_{\text{ND},m} \tilde{\mathbf{\Lambda}}_{\text{ND},m}^{-1} \right\} \right)^2}{\left( \text{tr} \left\{ \mathbf{\Lambda}_{\text{ND},m} \right\} \right)^2}.
\end{aligned} \tag{85}$$

The clutter power after filtering with (84) is found from (41) to be

$$\begin{aligned}
R_{o,\text{SDP-LDF}} &= \sigma_x^2 \mathbf{w}_{\text{SDP-LDF},k}^H \mathbf{V} \mathbf{\Lambda} \mathbf{V}^H \mathbf{w}_{\text{SDP-LDF},k} \\
&= \sigma_x^2 \frac{\text{tr} \left\{ \mathbf{\Lambda}_{\text{ND},m}^2 \tilde{\mathbf{\Lambda}}_{\text{ND},m}^{-2} \right\}}{\text{tr} \left\{ \mathbf{\Lambda}_{\text{ND},m} \right\}}.
\end{aligned} \tag{86}$$

The noise power is then similarly found from (84) and (42):

$$\begin{aligned}
N_{o,\text{SDP-LDF}} &= \sigma_u^2 \mathbf{w}_{\text{SDP-LDF},k}^H \mathbf{w}_{\text{SDP-LDF},k} \\
&= \sigma_u^2 \frac{\text{tr} \left\{ \mathbf{\Lambda}_{\text{ND},m} \tilde{\mathbf{\Lambda}}_{\text{ND},m}^{-2} \right\}}{\text{tr} \left\{ \mathbf{\Lambda}_{\text{ND},m} \right\}}.
\end{aligned} \tag{87}$$

Equations (85)-(87) are then combined to find the output SINR from LDF filtering of the SDP symbol as

$$\begin{aligned}
\text{SINR}_{o,\text{SDP-LDF}}(m) &= \\
&= \frac{|\alpha|^2 \left( \text{tr} \left\{ \mathbf{\Lambda}_{\text{ND},m} \tilde{\mathbf{\Lambda}}_{\text{ND},m}^{-1} \right\} \right)^2}{\text{tr} \left\{ \mathbf{\Lambda}_{\text{ND},m} \right\} \left( \sigma_x^2 \text{tr} \left\{ \mathbf{\Lambda}_{\text{ND},m}^2 \tilde{\mathbf{\Lambda}}_{\text{ND},m}^{-2} \right\} + \sigma_u^2 \text{tr} \left\{ \mathbf{\Lambda}_{\text{ND},m} \tilde{\mathbf{\Lambda}}_{\text{ND},m}^{-2} \right\} \right)},
\end{aligned} \tag{88}$$

resulting in a processing gain of

$$\begin{aligned}
\Delta_{\text{SDP-LDF}}(m) &= \\
&= \frac{NM(\sigma_x^2 + \sigma_u^2) \left( \text{tr} \left\{ \mathbf{\Lambda}_{\text{ND},m} \tilde{\mathbf{\Lambda}}_{\text{ND},m}^{-1} \right\} \right)^2}{\text{tr} \left\{ \mathbf{\Lambda}_{\text{ND},m} \right\} \left( \sigma_x^2 \text{tr} \left\{ \mathbf{\Lambda}_{\text{ND},m}^2 \tilde{\mathbf{\Lambda}}_{\text{ND},m}^{-2} \right\} + \sigma_u^2 \text{tr} \left\{ \mathbf{\Lambda}_{\text{ND},m} \tilde{\mathbf{\Lambda}}_{\text{ND},m}^{-2} \right\} \right)}.
\end{aligned} \tag{89}$$



**Justin Metcalf** (S'08) received the Bachelors degree in Computer Engineering from Kansas State University in 2006. From 2006-2008 he was at the Flight Simulation Labs of Lockheed Martin Aeronautics in Fort Worth, TX. From 2008-2014 he was with the Radar Systems & Remote Sensing Lab of the University of Kansas, where he obtained a Masters degree in Electrical Engineering (with Honors) in 2011 and the Ph.D. degree in Electrical Engineering (with Honors) in 2015. He was the recipient of the Richard and Wilma Moore Award for the best departmental Masters thesis in 2011-2012. In 2014 Dr. Metcalf joined the Sensors Directorate of the Air Force Research Laboratory as a Research Electronics Engineer.



**Cenk Sahin** (S'06) received the B.S. degree (*summa cum laude*) in electrical and computer engineering from University of Missouri-Kansas City, Kansas City, MO in 2008 and the M.S. degree (*with honors*) in electrical engineering from University of Kansas, Lawrence, KS in 2012. Currently, he is a Ph.D. candidate in electrical engineering at the University of Kansas. His general research interests include digital communication theory, information theory, queueing theory, and their application to wireless communication systems.



**Shannon D. Blunt** (S96M02SM07) received the Ph.D. degree in electrical engineering from the University of Missouri in 2002. From 2002 to 2005 he was with the Radar Division of the Naval Research Laboratory in Washington, D.C. Since 2005 he has been with the Department of Electrical Engineering and Computer Science at the University of Kansas where he is currently a Professor and Director of the Radar Systems & Remote Sensing Lab (RSL).

In 2012 Prof. Blunt received the IEEE/AESS Nathanson Memorial Radar Award and in 2008 received the AFOSR Young Investigator Award. He has over 100 refereed journal and conference publications, 11 patents, 5 book chapters, and co-edited the book Principles of Waveform Diversity & Design.

He is a member of the IEEE/AESS Radar Systems Panel where he is currently Chair of the Conferences Committee. He is an Associate Editor for IEEE Transactions on Aerospace & Electronic Systems and is on the Editorial Board for IET Radar, Sonar & Navigation. He was General Chair of the 2011 IEEE Radar Conference in Kansas City and is a member of the program committee for the MSS Tri-Service Radar Symposium series. He was Chair of the NATO SET-179 research task group on Dynamic Waveform Diversity & Design and a member of SET-182 on Radar Spectrum Engineering & Management and SET-227 on Cognitive Radar. He is a Senior Member of IEEE.



**Muralidhar Rangaswamy** (S89, M93, SM98, F2006) received the B.E. degree in Electronics Engineering from Bangalore University, Bangalore, India in 1985 and the M.S. and Ph.D. degrees in Electrical Engineering from Syracuse University, Syracuse, NY, in 1992. He is presently employed as the Senior Advisor for Radar Research at the RF Exploitation Branch within the Sensors Directorate of the Air Force Research Laboratory (AFRL). Prior to this he has held industrial and academic appointments.

His research interests include radar signal processing, spectrum estimation, modeling non-Gaussian interference phenomena, and statistical communication theory. He has co-authored more than 200 refereed journal and conference record papers in the areas of his research interests. Additionally, he is a contributor to 8 books and is a co-inventor on 3 U.S. patents.

Dr. Rangaswamy is the Technical Editor (Associate Editor-in-Chief) for Radar Systems in the IEEE Transactions on Aerospace and Electronic Systems (IEEE-TAES). He served as the Co-Editor-in-Chief for the Digital Signal Processing journal between 2005 and 2011. Dr. Rangaswamy serves on the Senior Editorial Board of the IEEE Journal of Selected Topics in Signal Processing (Jan 2012-Dec 2014). He was a 2 term elected member of the sensor array and multichannel processing technical committee (SAM-TC) of the IEEE Signal Processing Society between January 2005 and December 2010 and serves as a member of the Radar Systems Panel (RSP) in the IEEE-AES Society. He was the General Chairman for the 4th IEEE Workshop on Sensor Array and Multichannel Processing (SAM-2006), Waltham, MA, July 2006. Dr. Rangaswamy has served on the Technical Committee of the IEEE Radar Conference series in a myriad of roles (Track Chair, Session Chair, Special Session Organizer and Chair, Paper Selection Committee Member, Tutorial Lecturer). He served as the Publicity Chair for the First IEEE International Conference on Waveform Diversity and Design, Edinburgh, U.K. November 2004. He presently serves on the conference sub-committee of the RSP. He was the Technical Program Chairman for the 2014 IEEE Radar Conference.

He received the IEEE Warren White Radar Award in 2013, the 2013 Affiliate Societies Council Dayton (ASC-D) Outstanding Scientist and Engineer Award, the 2007 IEEE Region 1 Award, the 2006 IEEE Boston Section Distinguished Member Award, and the 2005 IEEE-AESS Fred Nathanson memorial outstanding young radar engineer award. He was elected as a Fellow of the IEEE in January 2006 with the citation for contributions to mathematical techniques for radar space-time adaptive processing. He received the 2012 and 2005 Charles Ryan basic research award from the Sensors Directorate of AFRL, in addition to more than 40 scientific achievement awards.